AD-A170 644 TESTS AND INTERPRETATION OF MIXED MODE I AND II FULLY PLASTIC FRACTURE FR..(U) MASSACHUSETTS INST OF TECH CAMBRIDGE DEPT OF MECHANICAL ENGIN.. 1/1

UNCLASSIFIED G A KARDOMATEAS ET AL. 31 JUL 86 F/G 11/6 NL

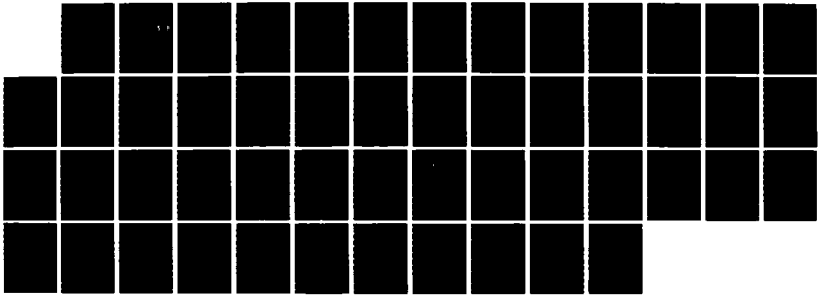

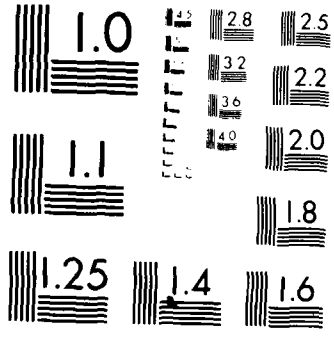

MICROCOPY RESOLUTION TEST CHART
NATIONAL BUREAU OF STANDARDS 1963-A

(1)

Technical Report N00014-82-K-0025 P00002 TR06

TESTS AND INTERPRETATION OF MIXED MODE I AND II FULLY PLASTIC FRACTURE FROM SIMULATED WELD DEFECTS

George A. Kardomateas
General Motors Research Laboratories
Engineering Mechanics Department
Warren, MI 48090-9055

Frank A. McClintock
Room 1-304, (617) 253-2219
Department of Mechanical Engineering
Massachusetts Institute of Technology
Cambridge, MA 02139

Unlimited Distribution

31 July, 1986

Technical Report

Prepared for
OFFICE OF NAVAL RESEARCH
Solids Mechanics Program, Mechanics Division
Scientific Officer: Dr. Yapa Rajapakse
Code 4335 (202) 696-4306
800 N. Quincy Street
Arlington, VA 22217

SECURITY CLASSIFICATION OF THIS PAGE (When Data Entered)

REPORT DOCUMENTATION PAGE		READ INSTRUCTIONS BEFORE COMPLETING FORM
1. REPORT NUMBER N00014-82-K-0025 P00002 TR06	2. GOVT ACCESSION NO.	3. RECIPIENT'S CATALOG NUMBER
4. TITLE (and Subtitle) TESTS AND INTERPRETATION OF MIXED MODE I AND II FULLY PLASTIC FRACTURE FROM SIMULATED WELD DEFECTS		5. TYPE OF REPORT & PERIOD COVERED Technical Report 31 July 1986 6. PERFORMING ORG. REPORT NUMBER
7. AUTHOR(s) Frank. A. McClintock George A. Kardomateas (now at General Motors Lab Eng.Mech.Dept., Warren MI 48090-9055		8. CONTRACT OR GRANT NUMBER(s) N00014-82-K-0025 P00002
9. PERFORMING ORGANIZATION NAME AND ADDRESS Department of Mechanical Engineering Massachusetts Institute of Technology Cambridge, MA 02139		10. PROGRAM ELEMENT, PROJECT, TASK AREA & WORK UNIT NUMBERS
11. CONTROLLING OFFICE NAME AND ADDRESS Office of Naval Research Solid Mechanics Program, Mech. Div. Code 432S 800 N. Quincy Street, Arlington, VA 22217		12. REPORT DATE 31 July 1986 13. NUMBER OF PAGES 42
14. MONITORING AGENCY NAME & ADDRESS(if different from Controlling Office)		15. SECURITY CLASS. (of this report) Unclassified 15a. DECLASSIFICATION/DOWNGRADING SCHEDULE
16. DISTRIBUTION STATEMENT (of this Report) Distribution Unlimited		
17. DISTRIBUTION STATEMENT (of the abstract entered in Block 20, if different from Report)		
18. SUPPLEMENTARY NOTES		
19. KEY WORDS (Continue on reverse side if necessary and identify by block number) Ductile fracture, fully plastic, mixed mode, crack initiation, crack growth, Mode I, Mode II, asymmetry, crack ductility, weld defects, experiments, shear lip, strain hardening, crack opening angle, crack tip displacement, tearing modulus, 1018, HY-80, HY-100		

20. ABSTRACT (Continue on reverse side if necessary and identify by block number)

Most fracture tests use symmetric specimens, with the crack advancing into the relatively undamaged region between two plastic zones. A crack near a weld or shoulder, loaded into the plastic range, may have only a single shear band, however, alnong which the crack grows into prestrained and damaged material with less ductility than the usual symmetric configurations. Tests on six alloys show that the crack growth ductility, defined as the minimum displacement per unit ligament reduction, is less in the asymmetric case

DD FORM 1 JAN 73 1473 EDITION OF 1 NOV 65 IS OBSOLETE

S N 0102-LF-014-6601

SECURITY CLASSIFICATION OF THIS PAGE (When Data Entered)

than in the symmetric one by a factor of 3 for low-hardening alloys (with strain hardening exponents n = 0.1). This means that with low-hardening (typically high strength) alloys, the surrounding structure must be 3 times stiffer for fracture-stable design. For higher hardening alloys (n = 0.23) the crack growth ductility is less in the asymmetric case by a factor of at most 1.2. The crack initiation ductility (here approximately the crack tip displacement CTD) is relatively unaffected by asymmetry, but it cannot always be relied on for ductility, (e.g. in low cycle fatigue). Therefore tests such as these on crack growth ductility are needed for help in design and maintenance of structures.

Triaxiality on one side of the asymmetric shear crack diverts it from 45^{o} to 38^{o}-41^{o} (from the transverse direction), the smaller diversion with less strain hardening. In addition, the far field displacement vector is 51^{o} to 65^{o} from transverse, more with high hardening, suggesting a Mode I component even where the non-hardening slip line field predicts a pure shear displacement.

TESTS AND INTERPRETATION OF MIXED MODE I AND II FULLY PLASTIC FRACTURE FROM SIMULATED WELD DEFECTS

G.A. KARDOMATEAS* and F.A. McCLINTOCK

Department of Mechanical Engineering,
Massachusetts Institute of Technology, Cambridge MA 02139 USA

*Present address: Engineering Mechanics Dept., General Motors Research Laboratories, Warren MI 48090-9055 USA

TABLE OF SYMBOLS

COA	crack opening angle, Fig. 5
D_{ext}	minimum extension rate, Eq. 10
D_g	crack growth ductility, Eq. 7
E	modulus of elasticity, Eq. 11
F_L	load factor, Eq. 5
J	J-integral, Eq. 12
k	shear yield strength, Eq. 1
l_0	initial projected ligament, Eq. 4
l_l	projected length of lower crack flank, Eq. 8, Fig. 5
n	strain hardening exponent, Eq. 3
P_{nom}	limit load (with no strain hardening), Eq. 4
T.S.	tensile strength, Eq. 4
T	tearing modulus, Eq. 11
T^*_{asym}	modified tearing modulus, Eq. 14
u_i	initiation displacement, Fig. 4, Eq. 1
u_g	crack growth displacement, Eq. 6
$\vec{v}_l$	total displacement vector, Fig. 6
$\vec{v}_g$	crack growth displacement vector, Fig. 6
w	specimen width, Eq. 4
Y.S.	tensile yield strength
γ_c	fracture strain, Eq. 1
θ_c	average crack direction from transverse, $(\theta_u+\theta_l)/2$
$\theta_{l,u}$	lower and upper flank angles from transverse, Figs. 5, 6
ρ	mean inclusion spacing, Eq. 1

$\bar{\sigma}_1$ flow strength at unit strain, Eqs. 1, 3

ϕ displacement angle from transverse, Figs. 5, 7a, 8a

ABSTRACT

Most fracture tests use symmetric specimens, with the crack advancing into the relatively undamaged region between two plastic shear zones. A crack near a weld or shoulder, loaded into the plastic range, may have only a single shear band, however, along which the crack grows into prestrained and damaged material with less ductility than the usual symmetrical configurations. Tests on six alloys show that the crack growth ductility, defined as the minimum displacement per unit ligament reduction, is less in the asymmetric case than in the symmetric one by a factor of 3 for low-hardening alloys (with strain hardening exponents $n \approx 0.1$). This means that with low-hardening (typically high strength) alloys, the surrounding structure must be 3 times stiffer for fracture-stable design. For higher hardening alloys ($n \approx 0.23$) the crack growth ductility is less in the asymmetric case by a factor of at most 1.2. The crack initiation ductility (here approximately the crack tip displacement CTD) is relatively unaffected by asymmetry, but it cannot always be relied on for ductility, (e.g. in low cycle fatigue). Therefore tests such as these on crack growth ductility are needed for help in design and maintenance of structures.

Triaxiality on one side of the asymmetric shear crack diverts it from 45° to 38°-41° (from the transverse direction), the smaller diversion with less strain hardening. In addition, the far field displacement vector is 51° to 63° from transverse, more with high hardening, suggesting a Mode I component even where the non-hardening slip line field predicts a pure shear displacement.

1. INTRODUCTION

For fracture-stable structures it is important not only that fully plastic conditions be attained before fracture, but also that the load not fall off too rapidly during crack growth. Flow fields such as that of Fig. 1, in which the far-field deformation consists of a single shear band, may arise in practice due to the constraint of weld material. These specimens may exhibit less ductility than the symmetric ones, because the crack is advancing into pre-strained and damaged material, rather than into the new material encountered by a crack advancing between two symmetrical shear bands. Being able to predict such increased crack growth can have useful applications in the design, inspection, and maintenance of pressure vessels and ships.

Observations show that ductile fracture results from a three-step process initiated by the cracking of inclusions or the separation of inclusion-metal interfaces, followed by hole growth to localization or coalescence. The coalescence of holes into a crack, which then grows by a similar mechanism, occurs either on a plane of high shear stress, giving elongated dimples, or on a plane normal to the direction of maximum tensile stress, giving equiaxed dimples, e.g. Hayden and Floreen [1], Beachem and Meyn [2].

Ductile or fully plastic fracture consists of an initiation stage, characterized by a crack tip opening displacement (CTOD), and a growth stage which, if stable, may be characterized by the crack tip opening displacement per unit crack growth d(CTOD)/da, e.g. Shih, et al. [3], Dawes [4], Chipperfield, et al. [5]. For small angles, d(CTOD)/da is the crack opening angle COA. Initiation has been

described by the path independent stress-displacement integral J, to which it is proportional. Crack growth is also described by the tearing modulus $T = dJ/da$, e.g. Paris, et al. [6], which is also approximately the crack opening angle COA divided by the elastic strain at the tensile strength, T.S./E. (These relations will both be derived below in Sec. 2b, Interpretation of Tests.)

In general, ductile fracture occurs by hole growth, which depends on the combined history of stress, strain, and rotation near the crack tip, where the holes are growing. The validity of a single measure for fracture, such as CTOD or J, depends on the presence of a stress-strain singularity near the crack tip that is governed by a single scalar quantity. For initiation the Hutchinson [7], Rice-Rosengren [8] (HRR) singularity indeed often dominates, as shown by finite element studies of McMeeking and Parks [9]. Such singular fields for growth seem to be available only for the elastic-plastic case, e.g. Slepyan [10], [11], Rice [12], and Ponte-Castaneda [13], [14]. They probably do not dominate when strains are large compared to the elastic strain all across a section, from the hole growth in the fracture process zone to the far boundary. Nonetheless, data are often presented as if a single dominant singularity existed, or perhaps in the hope that it does. For instance, typical values of d(CTOD)/da for various bend tests are given in Table 1. In the limit of no strain hardening, it is well known that a variety of stress and strain states exist at the crack tip, depending on the geometry and mode of loading, e.g. McClintock [16]. Reduced ductility has been shown in a configuration giving a high strain concentration, even at the expense of reduced triaxiality, e.g. McClintock [17]. It is the possibility of unexpectedly low ductility in such practical configurations as that of Fig. 1 that concerns us here. As Paris et al. [6] have shown, low crack growth ductility can lead to instability of structures.

The fractography of pure Mode II loading was studied by Jones and Chisholm [18]. The ductility in pure Mode II loading was measured by Chant et al. [19] on high hardening carbon manganese steel (B.S. 1501-151-430A, Y.S. = 329 MN/m^2, T.S. = 490 MN/m^2). They found the ductility, measured by dJ/da, to be practically the same in Mode II and Mode I, although the microscopic features were different for the two modes. The tests described here deal with Mode II deformation under combined Mode I and II loading, as is found in asymmetric crack configurations in plates, near welds or shoulders (Fig. 1).

Near the tip of the growing crack, strain hardening causes the deformation field to fan out. For power law creep or deformation theory plasticity, the stress and strain in the neighborhood of a stationary crack can be found from Shih's mixed mode solutions [20]. For a growing crack, a fully-plastic, incremental plasticity solution should be obtained, taking into account the hardening of the material left behind the growing crack. Pending such an analysis, McClintock and Slocum [21] used a superposition of strain increments adapted from Shih's analysis. The crack was assumed to follow the center of the 45° shear band. The axial displacement for initiation, u_i, with a band at ϕ from the transverse direction is given in terms of the flow stress at unit strain $\bar{\sigma}_1$, the shear yield strength k, the mean inclusion spacing ρ, the critical fracture strain γ_c, and the strain hardening exponent n:

$$u_i = \frac{\bar{\sigma}_1}{k} I_{1/n} \rho \left(\frac{\gamma_c}{2\tilde{\epsilon}} \right)^{n+1} \sin \phi . \qquad (1)$$

For the assumed pure Mode II deformation, $\tilde{\epsilon} = 0.88$. For n = 0.1-0.2, $I_{1/n}$ = 0.72-0.83. For $\bar{\sigma}_1/k = 3$ and $\gamma_c = 0.8$, the initiation displacement is of the order of the inclusion spacing ($\rho \approx 0.01$ mm). For a quasi-steady growth, the crack advance per unit displacement was practically insensitive to the strain hardening

exponent n:

$$\frac{d(u/u_i)}{d(c/\rho)} = \frac{n+1}{\ln[(c-c_i)/\rho + \exp(n+1)]} . \qquad (2)$$

The above formula, for a mean inclusion spacing ρ =0.01 mm and crack growth over the ligament length of $l_0 = 2.54$ mm, gives du/dc ≈ 0.2.

To correct for triaxial effects around the crack tip, Kardomateas et al. [22], considered several sites around the current crack tip. The damage at each site due to the deformation for crack initiation and prior growth was determined and then the crack was grown in the direction requiring the least increment in far field displacement. While the results were generally as expected, some inconsistencies have appeared, so the results unfortunately cannot be relied on.

EXPERIMENTAL PROCEDURES

a. Material.

Tensile tests were performed on six alloys with the compositions and conditions listed in Table 1, using standard 6.35 mm dia. specimens with 25.4 mm gage length. Curves of true stress $\bar{\sigma}$ vs. integrated equivalent plastic strain $\bar{\epsilon}^p$ are represented by

$$\bar{\sigma} = \bar{\sigma}_1 (\epsilon_0 + \bar{\epsilon}^p)^n . \qquad (3)$$

The Bridgman correction for necking was applied with the ratio of net section radius a to profile radius R found from the empirical relation that it increases directly with the amount that the strain exceeds the uniform strain e.g. McClintock and Argon [23]: $a/R = \epsilon - \epsilon_u$.

The three constants $\bar{\sigma}_1$, ϵ_0 , and n were fitted three ways: to the yield strength YS , the tensile strength TS and the load maximum there, and the logarithmic (uniform) strain at the tensile strength ϵ_u ; to the

tensile strength conditions and the equivalent true strength and strain at fracture, σ_f and ϵ_f ; and to YS and the flow strengths taken rather arbitrarily at $\bar{\epsilon}^p = 0.125$ and $\bar{\epsilon}^p = 0.250$. The results fell in the range shown in Table 2. We denote as "lower hardening alloys" the 1018 cold finished, the HY-80, and the HY-100 steels ($n \approx 0.1$); and as "higher hardening alloys' the 1018 normalized and A36 hot rolled steels ($n \approx 0.2$). The 5086-H111 aluminum is between these two groups.

b) Test Method.

From 12.7 mm. dia. round bars of each alloy, seven specimens were first machined as shown in Fig. 3a, with side grooves to ensure a straight fatigue pre-crack approximately 1.3 mm deep with a root radius of 0.25 mm. For the four asymmetric specimens (Fig. 2b), further side grooves were machined at 40° from the transverse direction. This corresponded to the crack direction found in preliminary tests and helped to maintain plane strain conditions and to give planar cracks with straight fronts. For the three symmetric specimens, since the crack grows by alternating shear at ±45°, orthogonal triangles were machined, as shown in Fig. 2c.

Stability of the tests turned out to be an important consideration due to the high crack growth rate expected in the asymmetric case. Thus short specimens, stiff adapters, and locknuts were used. The tensile tests were performed on an 0.5 MN (50 metric ton) MTS testing machine with compliances of 2.3×10^{-6}, 4.6×10^{-6}, and 1.08×10^{-6} mm/N for the steel specimens, the adapters (including a pin-joint), and the machine, respectively. Stable tests were obtained except for the lower hardening alloys, which were dynamic for less than 20% of the falling part of the load-displacement curve.

The load was plotted continuously versus the axial displacement across the shoulders, as measured with a strain gauge extensometer. A strain gauge transverse displacement meter gave relative displacements between extension arms so that the measurement was made at the net section, as shown in Fig. 3.

c) Interpretation of Tests.

A typical plot of load vs. axial displacement is shown in Fig. 4. It can be idealized as a trapezoid consisting of an initial line corresponding to the elastic compliance across the 25 mm gauge length, a horizontal line at the maximum load, and a line tangent to the steepest part of the falling curve, associated with crack growth. The displacement corresponding to the horizontal line is called the idealized crack initiation displacement u_i^I. Since for a rigid-plastic material in this configuration the relative far-field displacement is the same as the crack tip displacement, the idealized initiation displacement is an approximation to the crack tip displacement. Although the plots like Fig. 4 were normalized by dividing by the gauge length, the crack-tip displacements for initiation are local quantities and should be independent of specimen size, so they will be given in terms of physical length. They are also then easier to compare with the more familiar crack tip opening displacements (CTOD) for Mode I.

The maximum load is normalized as the load factor, defined as the ratio of maximum load to a nominal load which is the limit load for a non-hardening material with the same tensile strength. For the single-edge-notch specimens tested here, the nominal load is given in terms of the initial projected ligament length l_0 after pre-cracking, the width w, and the tensile strength T.S. by

$$P_{nom} = l_0 w(T.S.)(2/\sqrt{3}) . \qquad (4)$$

Then the load factor F_L is

$$F_L = P_{max}/P_{nom} . \tag{5}$$

The most useful measure of the crack growth resistance seems to be the crack growth ductility D_g, defined as the minimum axial displacement per unit projected ligament reduction. Thinning of the ligament from the far side in fully plastic flow makes the reduction in ligament, rather than the crack advance, more appropriate for describing load drop. To reduce the effects of compliance, a crack growth displacement du_g is taken to consist of the gauge displacement du and the elastic unloading du_{unl} as shown in Fig. 4:

$$du_g = du + du_{unl} . \tag{6}$$

The ligament reduction can be approximated from the relative load drop, and thus we define:

$$D_g \equiv \left(\frac{du_g/l_0}{dP/P_{max}} \right)_{min} \approx \left(\frac{du_g}{dl} \right)_{min} . \tag{7}$$

From Fig. 5 using the law of sines gives the relation of D_g to the crack opening angle:

$$\frac{l_l}{\cos \theta_l} \sin(COA) = \frac{u_g}{\sin \phi} \sin (\phi - \theta_l + COA) ,$$

$$D_g = \frac{u_g}{l_l} = \frac{\sin(COA) \sin \phi}{\cos \theta_l \sin (\phi - \theta_l + COA)} . \tag{8}$$

In addition, the crack growth ductility is the normalized compliance requirement for fracture-stable design:

$$\text{Compliance of surroundings} < D_g l_0/P_{max} . \tag{9}$$

If it is not convenient to measure the cracked compliance giving du_{unl}, an

extensometer ductility D_{ext} is defined as

$$D_{ext} \equiv \left(\frac{du/l_0}{dP/P_{max}}\right)_{min} \approx \left(\frac{du}{dl}\right)_{min} . \tag{10}$$

This definition includes the effect of the compliance in the shoulders and is thus smaller than D_g.

The crack growth ductility gives a parameter analogous to the tearing modulus of Paris et al. [6]. They defined the tearing modulus in terms of the yield or tensile strength σ_0, the modulus E, and the J-integral by:

$$T = \frac{E}{\sigma_0^2}\frac{dJ}{dc} . \tag{11}$$

To approximate the J-integral, consider the simple case of the far-field displacement taking place along a single shear band and express it in terms of the shear strength, k, and the displacement along the band $u\sqrt{2}$, breaking through to the back surface where the band is of thickness t. The J integral in terms of work per unit volume W, and traction T is

$$J = \int\left(W dx_2 - T_j \frac{\partial u_j}{\partial x_1} ds\right), \tag{12}$$

The only non-zero term occurs where the shear band breaks through the back surface along a distance $\Delta x_2 = t\sqrt{2}$, where $W = ku\sqrt{2}$:

$$J = \left(ku\sqrt{2}\right)\left(t\sqrt{2}\right) = 2ku . \tag{13}$$

Thus define a modified tearing modulus, T^*, analogous to the tearing modulus T by introducing (13) into (11). In terms of the tensile strength, $\sigma_0 \approx$ T.S. $\approx k\sqrt{3}$,

$$T^*_{asym} = \frac{E}{(T.S.)^2} 2k \frac{du}{dc} \approx \frac{E}{T.S.} \frac{2}{\sqrt{3}} D_g . \tag{14}$$

An identical expression holds for the symmetric case.

More accurate measurements of the displacements during crack initiation and growth, u_i and u_g, are found from the profiles of the two crack surfaces, plotted using a metallurgical microscope with a travelling stage. Numerous horizontal and vertical coordinates were recorded through two linear potentiometers driving an x-y recorder. A typical plot, as in Fig. 6, consists of the 60° notch, the fatigue crack (with some amount of deformation, $\vec{v}_1 - \vec{v}_2$), an initiation zone which shows some blunting, and a growth zone. The initiation displacement is $\vec{v}_1 - \vec{v}_g$. In addition, fracture profiles were used to obtain the crack opening angle, COA, the lower and upper flank angles, θ_l and θ_u, the average crack direction, $\theta_c = (\theta_u + \theta_l)/2$, and the orientation of the total displacement vector, ϕ, for the asymmetric case. The breakthrough displacement, when the fracture first breaks through the back surface and leaves shear lips at the sides, is given by the vertical component of $\vec{v}_1$, and is usually indicated by a *flattening of the load-extension curve.*

3. RESULTS AND DISCUSSION

Plots of load and transverse displacement versus axial displacement are shown in Figs. 7 and 8 for symmetric and asymmetric HY-100 and A36 HR steels, typical of low and high hardening alloys. The predominant features for these and the other alloys are summarized in Table 3, along with data obtained from the fracture surface profiles, such as shown in Figs. 9 and 10.

Before considering the results in detail, note the major results. For the low-hardening HY-100 steel, the falling part of the load-displacement curve for the asymmetric specimens (Fig. 7a) is much steeper than that of the symmetric

specimens (Fig. 7b). Thus the asymmetric specimens of HY-100 steel require a much stiffer surrounding structure for stability. For the high-hardening A36 HR steel, the load-deformation curves for the asymmetric specimens fall off only a little more steeply (Figs. 8a vs. 8b). This corresponds to the large decrease in the crack opening angle of the asymmetric vs. the symmetric specimens of the low-hardening HY-100 steel (Figs. 9a, 9b), compared to the negligible increase for the high-hardening A36 steel (Figs. 10a, 10b).

a) Initiation Ductility Measures

Idealized initiation displacement, u_i^I. As shown in Table 3, this experimentally convenient measure of the crack tip displacement is not appreciably different for the asymmetric and symmetric configurations. It is, however, dependent on strain hardening: for the higher hardening alloys it is two to four times that for the lower hardening ones.

Profile initiation displacement, u_i. This more accurate initiation displacement, from fracture surface profiles, is given in the next pair of rows of Table 3. It is about 0.5 of the idealized initiation displacement, although ratios as low as 0.3 and as high as 0.7 are found in cold-rolled vs. normalized 1018 steel.

Both experimental observations of initiation displacement are larger by an order of magnitude or more than the 0.01 mm dimple or crack nucleus spacing of (1), found using the Shih mixed mode strain hardening singularities but neglecting blunting. Similar results appear to be found by considering the effects of triaxiality around the crack tip but also neglecting blunting [22]. These results highlight the importance of taking blunting into account in any theoretical

calculations of crack initiation (e.g. McClintock [24], Rice and Johnson [25]).

Maximum load. In Table 3 the maximum load is characterized by the load factor of [17], which is the maximum load divided by the limit load of non-hardening material based on the tensile strength. The load factors are in general somewhat larger in the higher hardening alloys, where there is more strain-hardening around the initial notch, and for the symmetric cases, where more ductility allows higher strain-hardening.

Far-field displacement. In the asymmetric case, the angle o of the far-field displacement vector from the transverse direction, defined from the slope of the transverse vs. axial displacement curves such as Figs. 7a and 8a, is greater than 45° and larger in the higher hardening alloys. The final relative far-field displacement vector $\vec{v}_1$ at o_c, measured after fracture from the microscope profile plots (Fig. 6), is between 51° and 63°. It is larger for the higher hardening alloys. The fact that it is typically greater than 45° means that there is some Mode I (opening) component of the crack tip displacement, beyond that associated with cracking to one side of a single 45° shear band in non-strainhardening material.

Crack Direction. "Zig-zagging" of the fracture surface is the characteristic of the 5086-H111 aluminum symmetric specimens, where two slip planes are active and the crack grows by alternating shear. The wavelength increased from 50 to 200 μm as the crack grew. In the end the fracture turned into a shear lip. Symmetric specimens in the lower hardening alloys also often turned into asymmetric ones, following only one slip plane. In some instances, half of the specimen followed the +45° slip plane and half the -45° plane.

Except for such final shear lips, in the symmetric specimens the macroscopic crack direction was within 10° of transverse. In the asymmetric specimens, the crack progressed at an angle of about θ_c = 38-41° from the transverse (Table 3). Relative to the shear band as determined from the far-field displacement, the crack was more transverse by $\phi - \theta_c$ = 10-25°, the more the higher the hardening. This is perhaps because these far-field and the local crack tip displacement vectors measured from the surface profiles were in different directions, rather than being parallel. Furthermore, this deviation from the shear band direction is expected from the higher triaxiality to one side of the crack tip displacement vector.

d) Crack Growth Ductility Measures

Crack growth ductility. In the low hardening alloys, the asymmetric crack growth ductility is less than the symmetric one by a factor of more than 3. Thus these alloys have 3 times the stiffness requirements for stability. In the high hardening alloys, on the other hand, D_g is less for the asymmetric geometry by only a factor of 1.2, at most. Expressed another way, in the asymmetric case the crack growth ductility in the lower hardening alloys is about 2 times less than in the higher hardening alloys. In the symmetric case, on the other hand, the crack growth rate is practically insensitive to strain hardening.

Modified tearing modulus, T^*. The tearing modulus T of Paris et al. [6] is approximated from the crack growth ductility for the asymmetric and the symmetric cases. The asymmetric values are lower than the symmetric ones by factor of 2 to 3 for the low hardening alloys, compared to factors of only 1 to 1.5 for the high hardening ones.

Extension rate, D_{ext}. If it is inconvenient to obtain the compliance near the steepest fall in the load-displacement curve to find D, the extensometer ductility $D_{ext} = (du/dl)_{min}$ may be used. It is lower than the crack growth ductility by 0.02 to 0.05, with some tendency for the larger difference to occur with the larger ductilities. The difference emphasizes the difficulty of fracture-stable design, since the net-section compliance it represents would not normally be included in calculating the compliance of the surrounding structure.

Profile displacement during growth, u_g/l_0. The displacement during growth from initiation until the fracture breaks through the back of the specimen, u_g, can be found from the fracture surface profiles (Fig. 6). Its normalized value, u_g/l_0, is in general only 10 to 20% larger than the crack growth ductility (except 25% for the aluminum alloy), indicating the validity of both measures.

Crack opening angle, COA. In the HY-100 steel, notice from Fig. 9 the large reduction in the crack opening angle (COA) of the asymmetric case relative to that of the symmetric, whereas in the A36 steel of Fig. 11 the difference in the COA between the two geometries is not appreciable. In Table 3, the COA is estimated from the crack growth ductility using (8), and also is given as found from the fracture profiles. For the asymmetric specimens the estimated COA's are low by a factor of 1.2 to 1.5, whereas for the symmetric specimens, they are low by a factor of 1.5 to 2. With one exception the ranking is correct; the disagreement is apparently due to error in reading the angles from the profiles, in view of the excellent agreement between the crack growth ductility D_g and the profile displacements u_g/l_0.

Marking the crack front. In the large 38.1 mm dia. 5086-H111 aluminum

specimens, the crack front was marked by imposing unloading-loading cycles at selected points during crack advance. The spacing of these fatigue marks was measured with a stereo microscope at about 50x. The corresponding displacements were then obtained from the load-displacement curves, accurate to about 0.01 mm. Figures 11 a,b show the load-displacement curves and Fig. 12 the crack growth-displacement data. The corresponding crack growth ductility can be calculated from (7) as $\Delta u/(\Delta c + \Delta u)$. For the symmetrical specimens there is an acceleration of crack growth. The average D_g is found to be 0.22, while that from the last two points of Fig. 12 is 0.16, compared to the values for large specimens reported below of 0.165. For the asymmetrical specimens, the crack growth rate is constant at $D_g = 0.09$, compared to the experimental value of 0.108. This tends to confirm the validity of Eq. 7 for finding the crack growth ductility from the slope of the load-displacement curve.

Comparison with analysis. Equation (2) gives a crack growth ductility of about 0.2, relatively independent of strain hardening. This is close to the crack growth ductility in the higher hardening alloys, but overestimates that in the lower hardening alloys by a factor of two. Notice, however, that this analysis is based on pure Mode II deformation and a superposition of stationary singularities and does not take into account the hardening of the material left behind the growing crack. This indicates the need for a fully-plastic, incremental plasticity solution for a growing, mixed-mode crack in strain-hardening material, taking triaxiality into account.

The greater ductility of the symmetric, higher hardening specimens is also shown qualitatively by the higher ratio of sliding off to hole growth observed in electron fractographs [26].

e) Size effects

Results of tests on 38.1 mm diameter specimens of 5086-H111 aluminum are compared with those from the 12.7 mm specimens in Table 4. As expected, the crack tip opening displacement at initiation, $u_i = 0.19$mm, is almost exactly the same for the two sizes. The maximum load was 5% higher, for no apparent reason. The crack growth ductility, as indicated by the displacement for growth across the ligament, u_g/l_0, was only 4% less for the large specimens.

For the size effects predicted by (2), use the mean inclusion spacing of about 10 microns and find the ratio of the crack growth rate for the large to that for the small specimens:

$$\frac{(dc/du)_{large}}{(dc/du)_{small}} = \frac{\ln[(c-c_i)/\rho]_{large}}{\ln[(c-c_i)/\rho]_{small}} = \frac{\ln(762)}{\ln(254)} = 1.20 .$$

Thus the integration of stationary crack fields gives a size effect due to an increasing crack advance per unit displacement that is small, but still more than observed in these experiments. Eventually, for large enough parts to give elastic-plastic fracture, there will of course be a size effect.

4. CONCLUSIONS

1. In asymmetric configurations with only a single shear band (which can occur with cracks near welds for example), the crack progresses into prestrained material instead of the new material between the two shear bands of the symmetric case.

2. Specimens and a procedure to test the resulting effects on ductility have been developed and shown to be valid by a number of independent checks.

3. Experiments on six structural alloys have shown that the resulting reduction in crack growth ductility for high strength, low-hardening ($n = 0.1$) alloys is a factor of about 3. In the higher hardening alloys ($n = 0.2$) the reduction is no more than 20%.

4. The high crack growth rate of the asymmetric configuration leads to correspondingly higher stiffness requirements for fracture-stable design.

5. The initiation displacement for symmetric and asymmetric configurations is not much different, and was large compared to the displacement during growth. This ductility cannot always be counted on, however, for example in cracks growing by low cycle fatigue. Therefore the crack growth ductility should be measured and used in the design and maintenance of ductile structures.

In addition to the above major conclusions, there are several detailed ones.

6. Trebling the specimen size in 5086-H111 gave negligible size effect on

the displacement to crack initiation, as expected, and appeared to reduce the crack growth ductility only by 4%, less than the 20% expected.

7. The crack growth direction is 38°-41° from the transverse (instead of 45°), as qualitatively expected from triaxial effects. The larger angle is with less strain-hardening.

8. The average displacement vector is at about 51°-63° from the transverse. Angles greater than 45° suggest a Mode I deformation component.

Acknowledgements. The financial support of the Office of Naval Research, Contract N0014-82-0025, and the interest and encouragement of the Project Monitor, Dr. Y. Rajapakse, are both gratefully acknowledged. The donation of the Hy-80 and Hy-100 steels by A. Wiggs of DTNSRDC is much appreciated. Also, C. Beer and L.P. Pate were very helpful in editing and re-editing the manuscript through SCRIBE.

REFERENCES

1. Hayden H.W. and Floreen S. "Observations of Localized Deformation During Ductile Fracture" *Acta Met.* 17, (1969) 213-224.

2. Beachem C.D. and Meyn D.A. "Fracture by Microscopic Plastic Deformation Processes" *Fractography* ASTM STP 436, Am. Soc. Testing Mat. Philadelphia, (1968) 59-88.

3. Shih C.F., deLorenzi H.G., Andrews W.R. "Studies on Crack Initiation and Stable Crack Growth" *Elastic-Plastic Fracture* ASTM STP 668, Am. Soc. Testing Mat., Philadelphia, (1979) 65-120.

4. Dawes M.G. "Elastic-Plastic Fracture Toughness Based on COD and J Contour Integral Concepts" *Elastic-Plastic Fracture* ASTM STP 668, Am. Soc. Testing Mat., Philadelphia, (1979) 307-333.

5. Chipperfield C.G., Knott J.F. and Smith R.F. "Critical Crack Opening Displacement in Low Strength Steels" Third Intern. Congress on Fracture, Munich, April 1973, paper I-233.

6. Paris P.C., Tada H., Zahoor A., and Ernst H. "The Theory of Instability of the Tearing Mode of Elastic-Plastic Crack Growth" *Elastic-Plastic Fracture* ASTM STP 668, Am. Soc. Testing Mat., Philadelphia, (1979) 5-36.

7. Hutchinson J.W. "Singular Behavior of a Tensile Crack in a Hardening Material" *J. Mech. Phy. Solids* 16, (1968) 13-31. See also "Plastic Stress Fields at a Crack Tip", ibid, 337-347.

8. Rice J.R. and Rosengren G.F. "Plane Strain Deformation Near a Crack Tip in a Power Law Hardening Material" *J. Mech. Phy. Solids* 16, (1968) 1-12.

9. McMeeking R.M. and Parks D.M. "On Criteria for J-Dominance of Crack-Tip Fields in Large-Scale Yielding" *Elastic Plastic Fracture* ASTM STP 668, Am. Soc. Testing Mat., Philadelphia, (1979) 175-194.

10. Slepyan L.I. "Growing Crack During Plane Deformation of an Elastic-Plastic Body" *Mekhanika Tverdogo Tela* 9, no.1, (1974) 57-67.

11. Slepyan L.I. "Deformation at the Edge of a Growing Crack", *Mechanica Tverdogo Tela* 8, no.4, (1973) 139-148.

12. Rice J.R. "Elastic-Plastic Crack Growth" *Mechanics of Solids: Hill Anniversary Volume* H.G. Hopkins and M.J. Sewell, eds., Pergamon Press, Oxford, (1982) 539-562.

13. Ponte-Castañeda P. "Asymptotic Fields in Steady Crack Growth with Linear Strain-Hardening", MECH-69, Div. of Appl. Sci., Harvard Univ., Cambridge, MA, submitted to *J. Mech. Phy. Solids*, (1985).

14. Ponte-Castañeda P. "Asymptotic Fields of a Perfectly Plastic, Plane-Stress Mode II Growing Crack", MECH-70, Div. of Appl. Sci, Harvard Univ., Cambridge, MA, submitted as a Brief Note to *J. Appl. Mech.*, (1985).

15. Andrews W.R. and Shih C.F. "Thickness and Side Groove Effects on J and δ Resistance Curves For A533B Steel at 93°C" *Elastic-Plastic Fracture* ASTM STP 668, Am. Soc. Testing Mat., Philadelphia, (1979) 426-450.

16. McClintock F.A. "Plasticity Aspects of Fracture" *Fracture vol.3* H. Liebowitz, ed., Academic Press NY, (1971) 47-225.

17. McClintock F.A. "On Notch Sensitivity" *Welding J. Res. Suppl.* 26, (1961) 202-208.

18. Jones D.L. and Chisholm D.B. "A Fractographic Study of the Edge-Sliding Mode in Fracture Toughness Testing",*Fractography - Microscopic Cracking Processes* ASTM STP 600, Am. Soc. Testing Mat., Philadelphia, (1976) 235-248.

19. Chant M., Green G., Whatmough I.J., Williams D.C. "The First Large Shear Specimen Test" General Electricity Generating Board Report No. SSW/SSD/0250/R/83, Job No. 01-95 (1983).

20. Shih C.F. "Small Scale Yielding Analysis of Mixed Mode Plane Strain Crack Problems" *Fracture Analysis* ASTM STP 560, Am. Soc. Testing Mat., Philadelphia, (1974) 187-210.

21. McClintock F.A. and Slocum A.H. "Predicting Fully Plastic Mode II Crack Growth from an Asymmetric Defect" *Int. J. Frac. Mech.* 27, (1985) 49-62.

22. Kardomateas G.A., McClintock F.A., and Carter W.T. "Directional Effects in Asymmetric Fully Plastic Crack Growth" *J. Eng. Frac. Mech.* 21, (1985) 341-351.

23. McClintock F.A. and Argon A.S. eds. *Mechanical Behavior of Materials*, Addison-Wesley, Reading, MA, (1966) 324.

24. McClintock F.A. "Crack Growth in Fully Plastic Grooved Tensile Specimens" *Physics of Strength and Plasticity* A.S. Argon, ed., MIT Press, Cambridge MA, (1969) 307-326.

25. Rice J.R. and Johnson M.A. "The Role of Large Crack Tip Geometry Changes in Plane Strain Fracture" *Inelastic Behavior of Solids* M.F. Kanninen et al., eds., McGraw-Hill NY, (1970) 641-672.

26. Kardomateas G.A. "Fractographic Observations in Asymmetric and Symmetric Fully Plastic Crack Growth" *Scripta Met.* 20, (1986) 609-614.

Table 1. Typical values of crack tip opening displacement per unit crack growth for symmetrical tests. All fatigue pre-cracked.

Material	Test	d(CTOD)/da ≈ COA, radians	Ref.
A533B steel Y.S. = 440 MPa T.S. = 574 MPa	Compact tension 102 mm th. 93°C	0.205	[3], [15]
ASTM A471 rotor steel Y.S. = 931 MN/m^2 T.S. = 1021 MN/m^2	3-point bend 6x1x0.5 in a/W = 0.502	0.164*	[6]
Free-cutting mild steel, annealed	3-point bend 5-17 mm th.	0.300	[5]
BS 4360 Grade 50 steel Y.S. = 358 MN/m^2 T.S. = 518 MN/m^2	3-point bend 25 mm th.	0.250	[4]

* Taken to be tearing modulus times elastic strain at tensile strength, T = (T.S./E)

Table 2. Room temperature tensile and hardness data for the six alloys tested.

Yield strength, strain	Tensile strength, unif.strn	Hardness	RA	Fracture true strg, strn		Parameters in Eq. 3 strength	pre-strain	exponent
YS, ϵ_y	TS, ϵ_u	"HDP"		σ_f	ϵ_f	σ_1	ϵ_0	n
MPa, -	MPa, -	kgf/mm^2	%			MPa	-	-
1018 steel, (0.15-0.20% C, 0.60-0.90% Mn) cold finished								
560 0.002	614 0.02	183	75	760 0.70		800	0.072	0.12
(The above are typical values; tests being re-run)								
HY-80 steel, (0.18% C, 2-3.25% Ni, 0.10-0.40% Mn, 0.15-0.35% Si)								
648 0.002	745 0.13	209	71	1200	1.25	1030-1150	0.007-0.043	0.10-0.17
HY-100 steel, (0.20% C, 2.25-3.50% Ni, 0.10-0.40% Mn, 0.15-0.35% Si)								
772 0.002	869 0.072	248	71	1350	1.24	1100-1280	0.001-0.111	0.06-0.18
5086-H111 aluminum, (4% Mg, 0.4% Mn, 0.15% Cr)								
225 0.002	333 0.15	82	44	480	0.58	510-540	0.002-0.010	0.15-0.18
1018 steel, normalized 1700°F in argon								
351 UYP 305 0.026	457 0.17	107	70	830	1.19	690-770	-0.025-0.100	0.14-0.27
A36 steel, (0.29% max C, 0.60-0.90% Mn; not rolled								
411 UYP 327 0.032	469 0.24	90	68	880	1.14	800-840	-0.020-0.022	0.20-0.26

Table 3 Test Results

Averages of 3 symmetric and 4 asymmetric tests. (Ligament ℓ_0=2.5 mm)

Alloy	1018 CF	Hy-80	Hy-100	5086-H111	1018 Norm	A36 HR
n =	0.12	0.13	0.12	0.16	0.20	0.23
a) INITIATION DUCTILITY MEASURES						
Idealized Initiation Displacement, u_1^I, mm (Fig. 4)						
Sym	0.183	0.274	0.211	0.455	0.854	0.437
Asym	0.185	0.279	0.254	0.409	0.640	0.523
Profile Initiation Displacement, u_1, mm (Fig. 6)						
Sym	0.053	0.130	0.130	0.201	0.544	0.203
Asym	0.084	0.183	0.132	0.185	0.386	0.279
b) MAXIMUM LOAD						
Load Factor $F_L = P_{max}/\ell_0 w(T.S.)(2/\sqrt{3})$ (Eq. 4)						
Sym	1.02	1.16	1.15	1.19	1.24	1.21
Asym	0.88	1.05	1.06	1.12	1.15	1.20
c) DIRECTIONS: DISPLACEMENT AND CRACK GROWTH						
Relative Far-Field Displacement Direction, ϕ (Fig. 6)						
Sym			($\approx 90^0$)			
Asym	51^0	55^0	55^0	56^0	61^0	61^0
Crack Direction, $\theta_c = (\theta_u+\theta_\ell)/2$ (Fig. 7)						
Sym			($\approx 0^0$)			
Asym	41^0	40^0	40^0	40^0	38^0	38^0

Table 3. cont.

Alloy	1018 CF	Hy-80	HY-100	5086-H111	1018 Norm	A36 HR
n =	0.12	0.13	0.12	0.16	0.20	0.23

d) CRACK GROWTH DUCTILITY MEASURES

Crack Growth Ductility, $D_g \equiv (du_c/d\ell_0)/(dP/P_{max})_{min} \approx (du_c/d\ell)_{min}$ (Eq. 7)

Svm	0.233	0.320	0.354	0.166	0.258	0.192
Asvm	0.072	0.096	0.105	0.108	0.215	0.181

Modified Tearing Modulus, $T^* \equiv (E/\bar{\sigma}.)(2/\sqrt{3})D_g$ (Eq. 14)

Svm	90.9	107.9	107.8	43.6	144.3	108.8
Asvm	28.2	32.4	47.4	28.4	115.2	102.6

Extension Rate, $D_{ext} \approx (\Delta u/d\ell)_{min}$ (over 25mm gauge length) (Eq. 10)

Svm	0.199	0.285	0.299	0.120	0.237	0.165
Asvm	0.046	0.060	0.061	0.083	0.195	0.154

Profile Growth Displacement, u_g/ℓ_0 (Fig. 7)

Svm	0.262	0.362	0.404	0.278	0.317	0.254
Asvm	0.084	0.115	0.125	0.136	0.230	0.216

Crack Opening Angle from Crack Growth Ductility, COA, Eq. 8

Svm	13^o	18^o	20^o	9.5^o	15^o	11^o
Asvm	0.7^o	1.3^o	1.5^o	1.6^o	4.7^o	3.7^o

Profile Crack Opening Angle, $COA = \theta_\ell - \theta_u$ (Fig. 6)

Svm	18^o	26^o	28^o	18^o	24^o	20^o
Asvm	1^o	2^o	2^o	2^o	6^o	5^o

Table 4 Size Effect in 5086-H111 Aluminum Alloy

Initial Ligament, ℓ_0, mm	2.54	7.62
a) INITIATION DUCTILITY MEASURES		
Idealized Initiation Displacement, u_1^I, mm (Fig. 4)		
Sym	0.455	0.206
Asym	0.409	0.183
Profile Initiation Displacement, u_1, mm (Fig. 6)		
Sym	0.201	0.066
Asym	0.185	0.061
b) MAXIMUM LOAD		
Load Factor $F_L = P_{max}/\ell_0 w(T.S.)(2/\sqrt{3})$ (Eqs. 4, 5)		
Sym	1.19	1.21
Asym	1.12	1.18
c) DIRECTIONS: DISPLACEMENT AND CRACK GROWTH		
Relative Far-Field Displacement Direction, ϕ (Fig. 6)		
Sym	($\approx 90^0$)	
Asym	56^0	57^0
Crack Direction, $\theta_c = (\theta_u + \theta_\ell)/2$ (Fig. 6)		
Sym	($\approx 0^0$)	
Asym	40^0	40^0

Table 4. cont.

Initial Ligament, ℓ_0, mm	1.54	7.62

d) CRACK GROWTH DUCTILITY MEASURES

Crack Growth Ductility, $D_g \equiv (du_c/d\ell_0)/(dF/F_{max})_{min} \approx (du_c/d\ell)_{min}$ (Eq. 7)		
Svm	0.166	0.165
Hsvm	0.108	0.105
Modified Tearing Modulus, $T^* \equiv (E/T.S.)(2/\sqrt{3})D_g$ (Eq. 14)		
Svm	43.6	43.4
Hsvm	28.4	27.6
Extension Rate, $D_{ext} \approx (du/d\ell)_{min}$ (over 25 mm gauge length) (Eq. 10)		
Svm	0.120	0.118
Hsvm	0.082	0.080
Profile Growth Displacement, u_g/ℓ_0 (Fig. 6)		
Svm	0.272	0.280
Hsvm	0.138	0.133
Crack Opening Angle from Crack Growth Ductility, COA, Eq. 8		
Svm	9.5^o	
Hsvm	1.6^o	
Profile Crack Opening Angle, $COA = \theta_\ell - \theta_u$ (Fig. 6)		
Svm	16^o	
Hsvm	2^o	

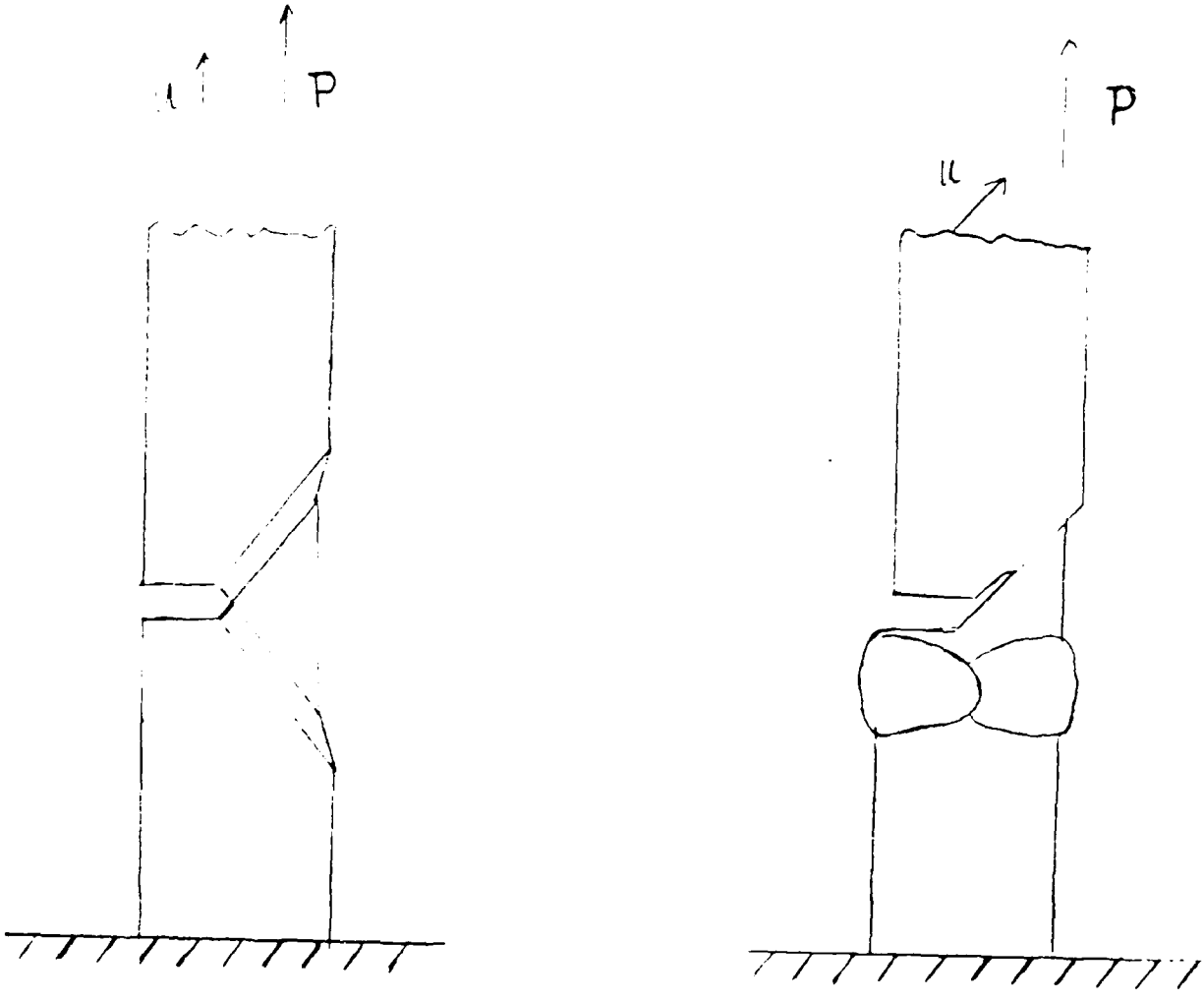

Fig. 1 Ideally plastic deformation of symmetric and asymmetric crack configurations.

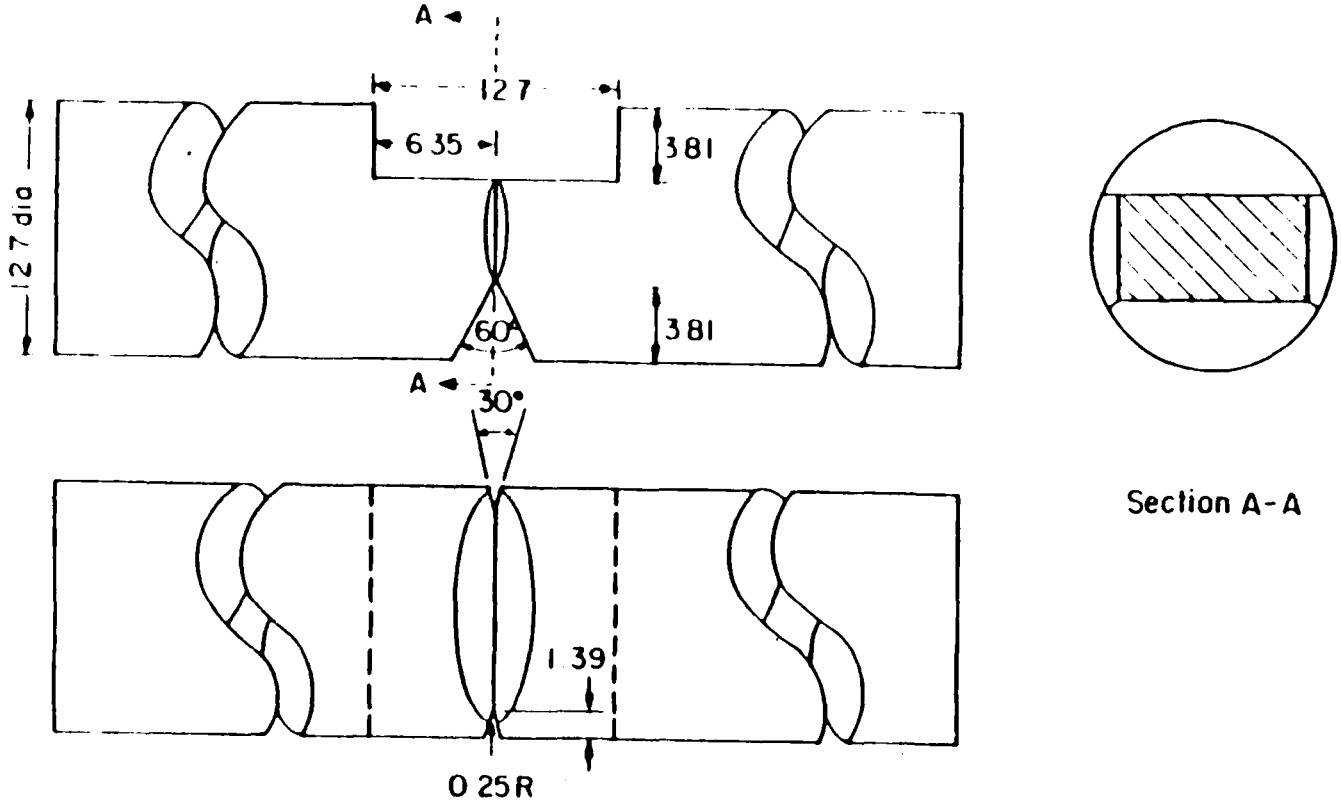

Figure 2a Machining for precracking of the specimens

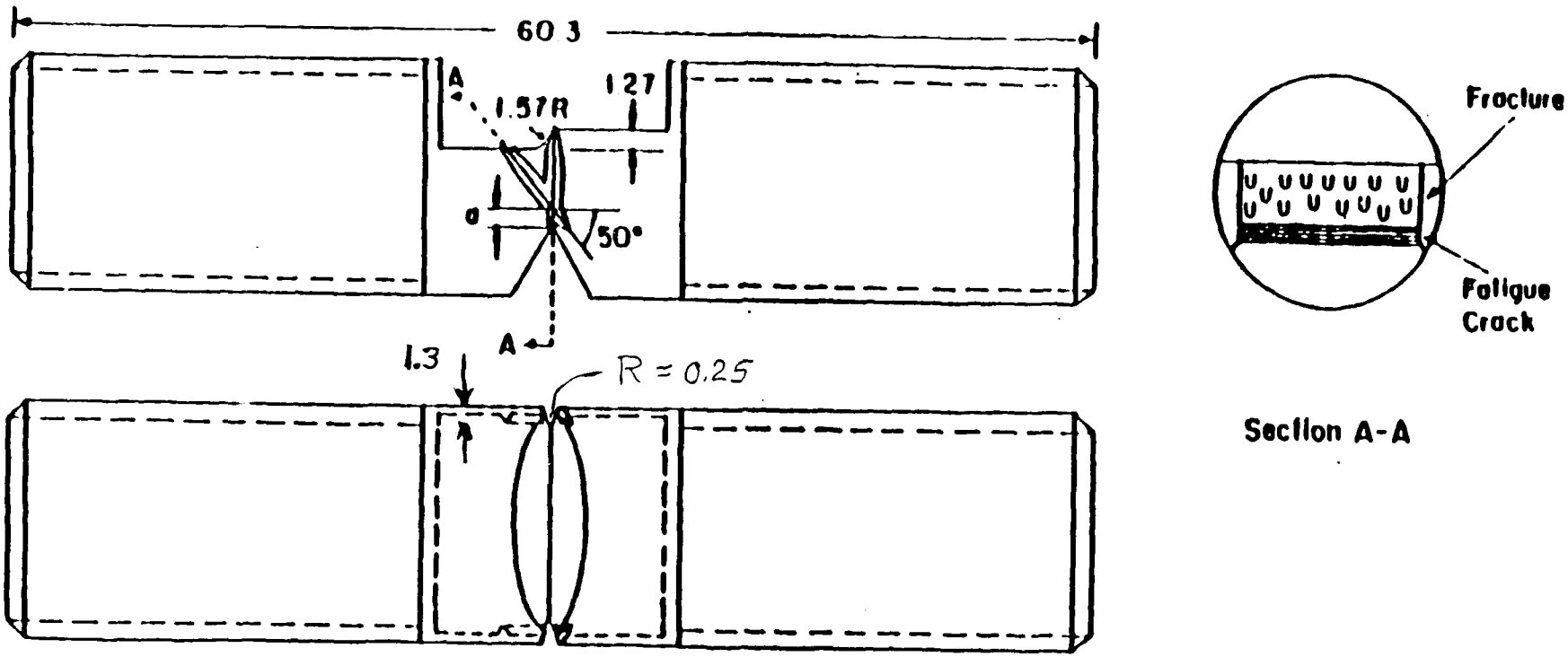

Figure 2b Second machining (after fatigue precracking) for the asymmetric specimens: a is the fatigue crack

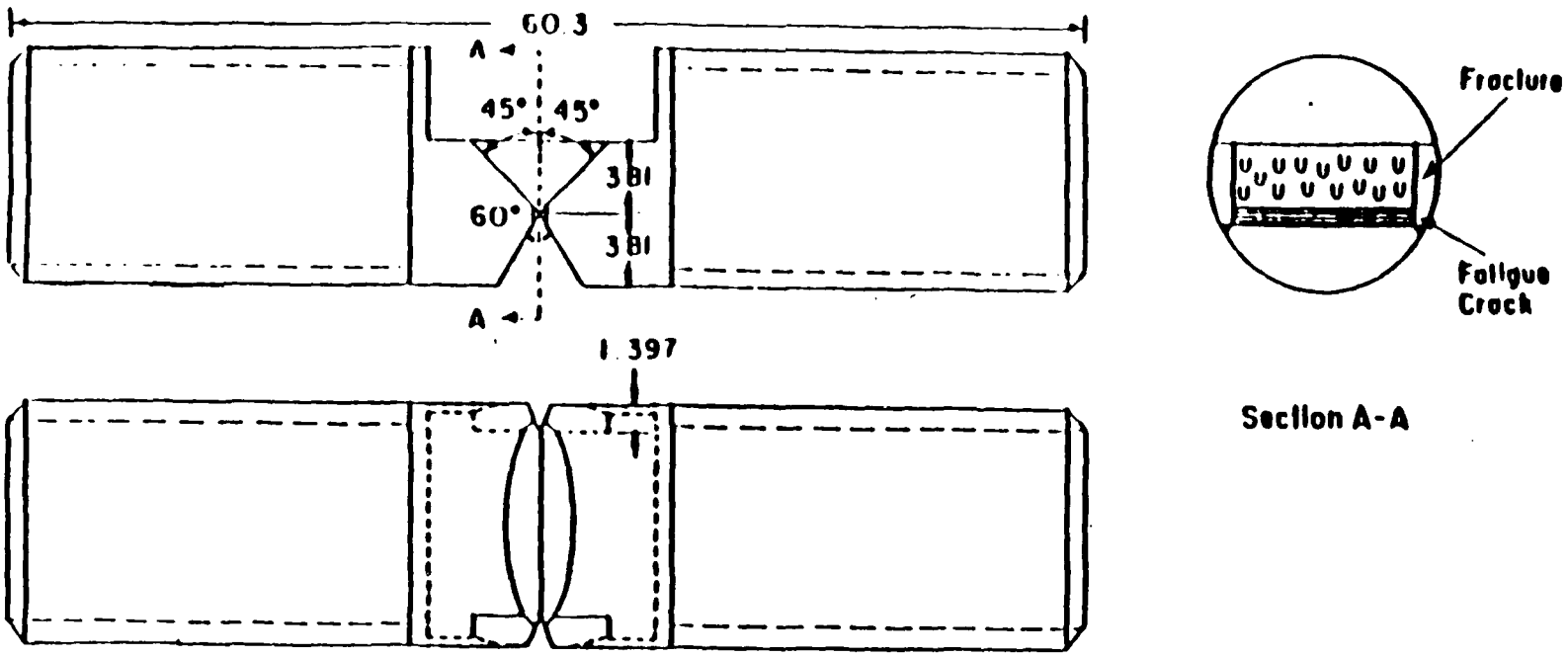

Figure 3c Second machining (after fatigue precracking) for the symmetric pecimens

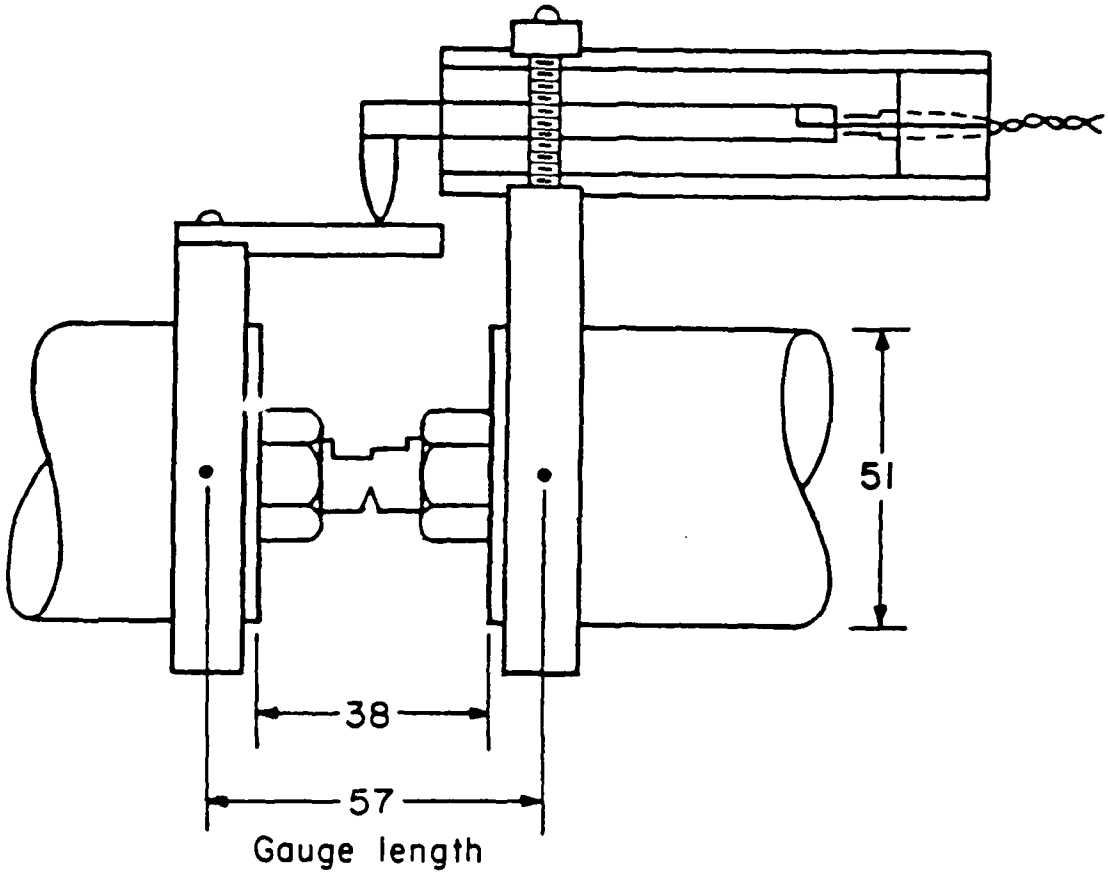

Fig. 3 Axial and transverse displacement gauge locations

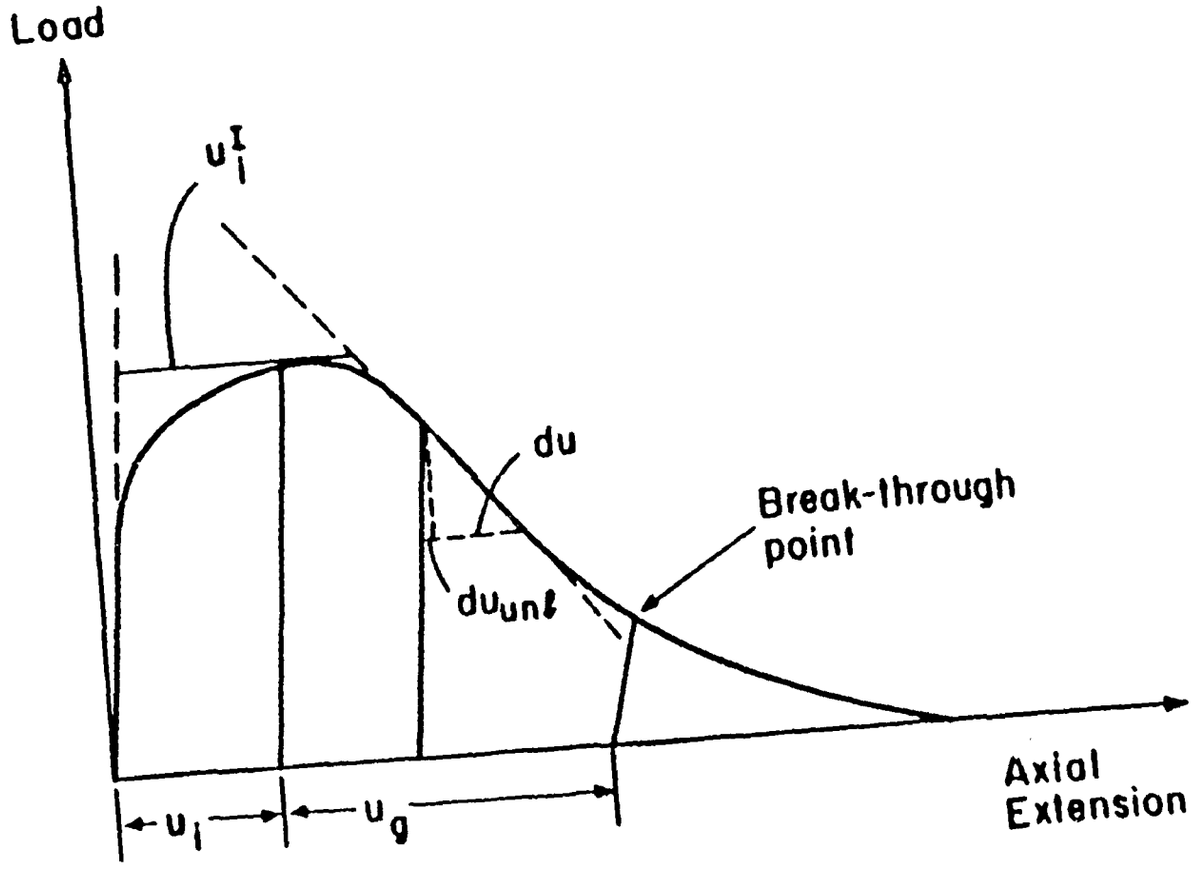

Figure 4 Schematic of the load vs axial gauge-point displacement curve. The displacements u_g and u_l are measured after fracture. The crack growth displacement is $du_c = du + du_{unl}$.

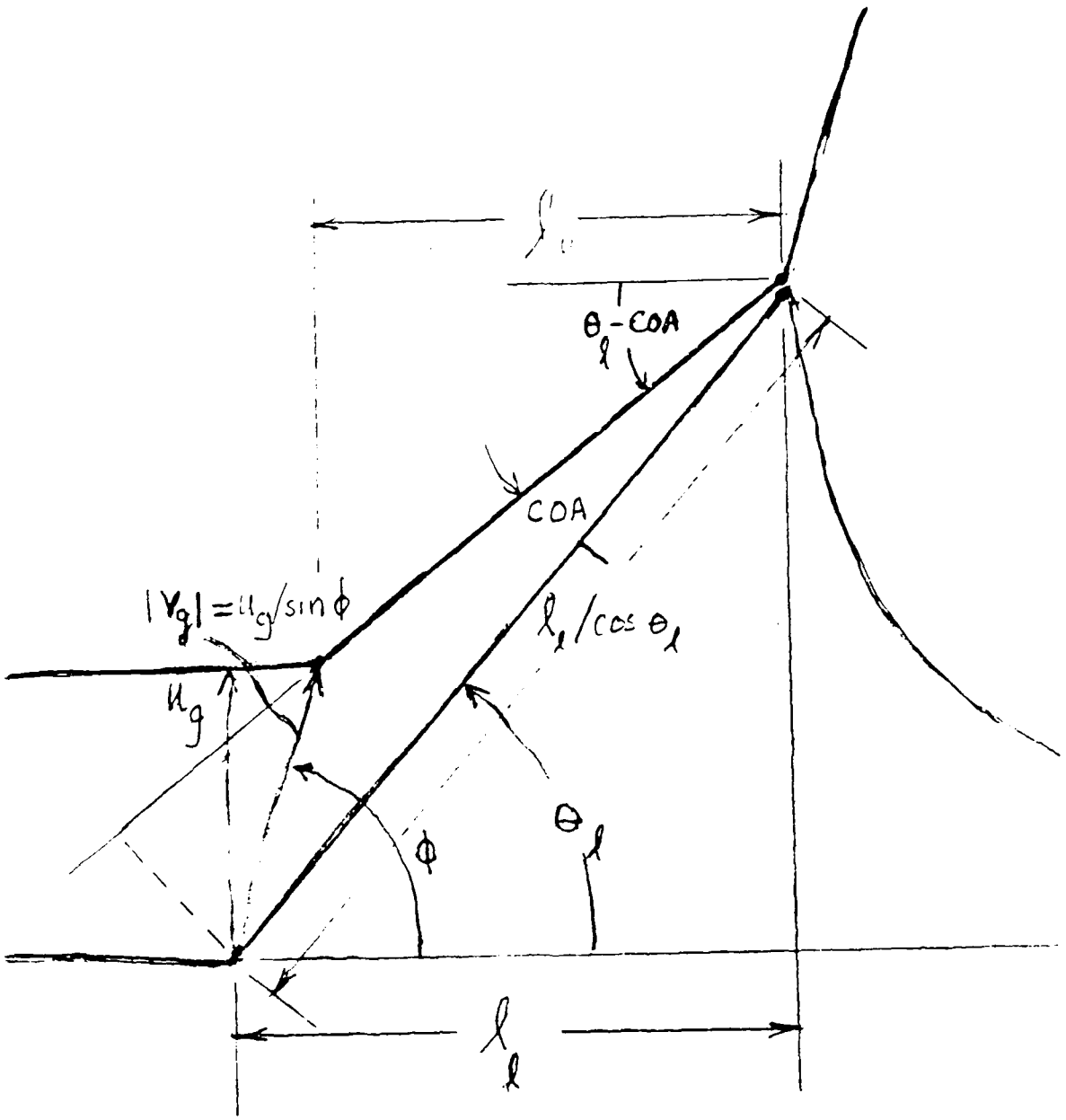

Figure 5. Deriving the relation between the crack opening angle and the crack growth rate

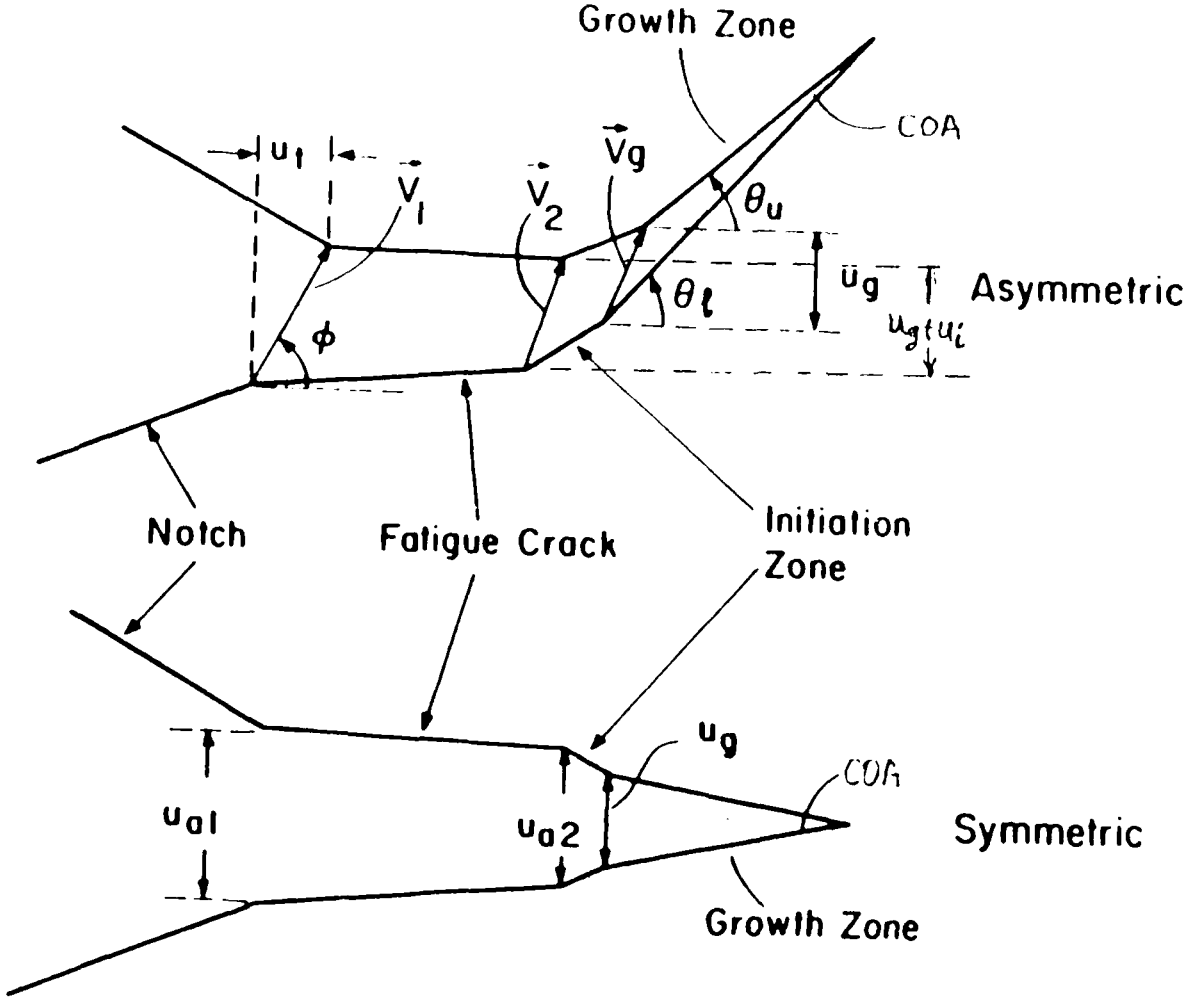

Figure 6. Schematic of the Fracture Surface Profile for the Asymmetric and Symmetric cases

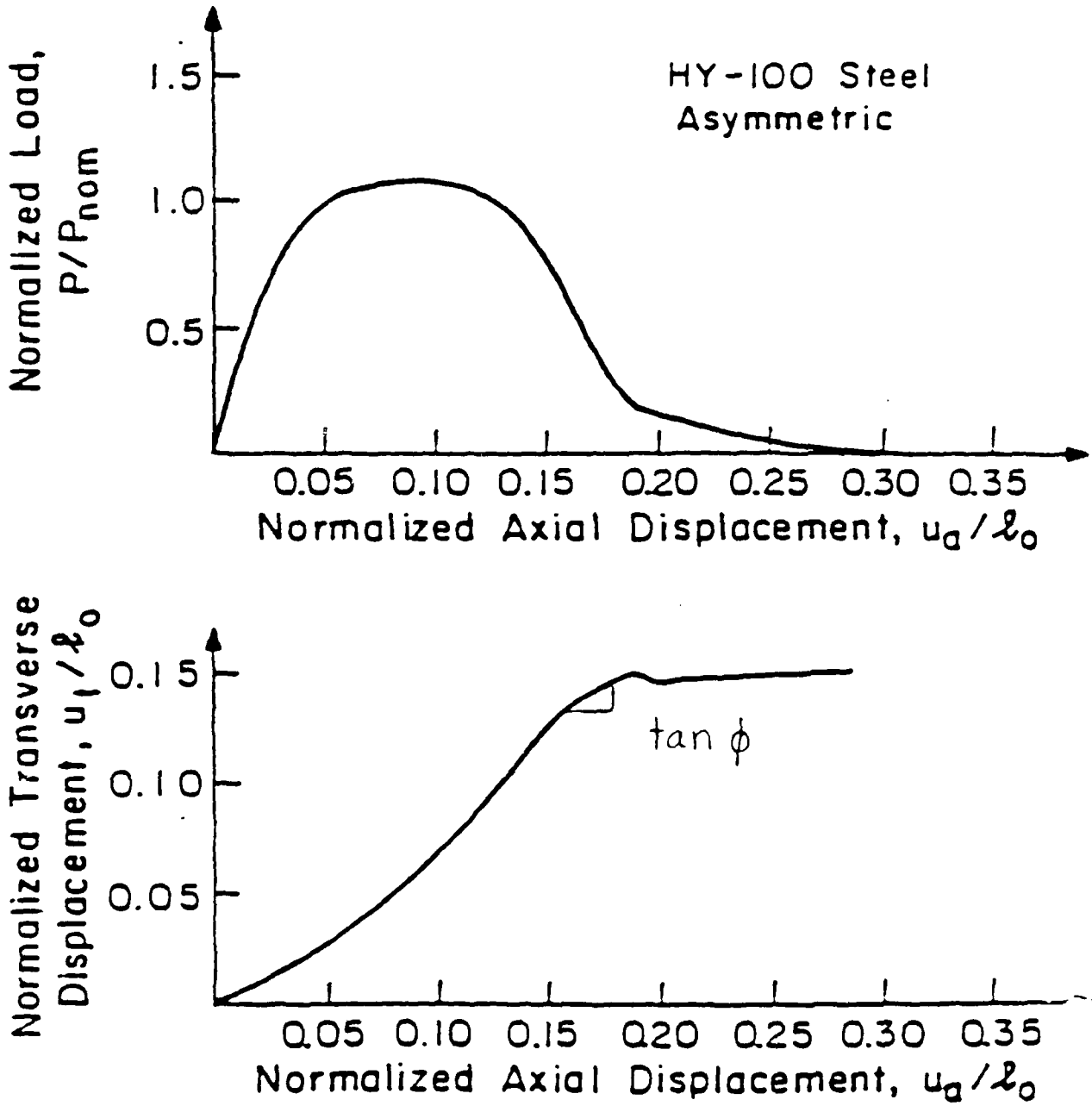

Figure 7a Test Data for the HY-100 Steel Asymmetric Specimens

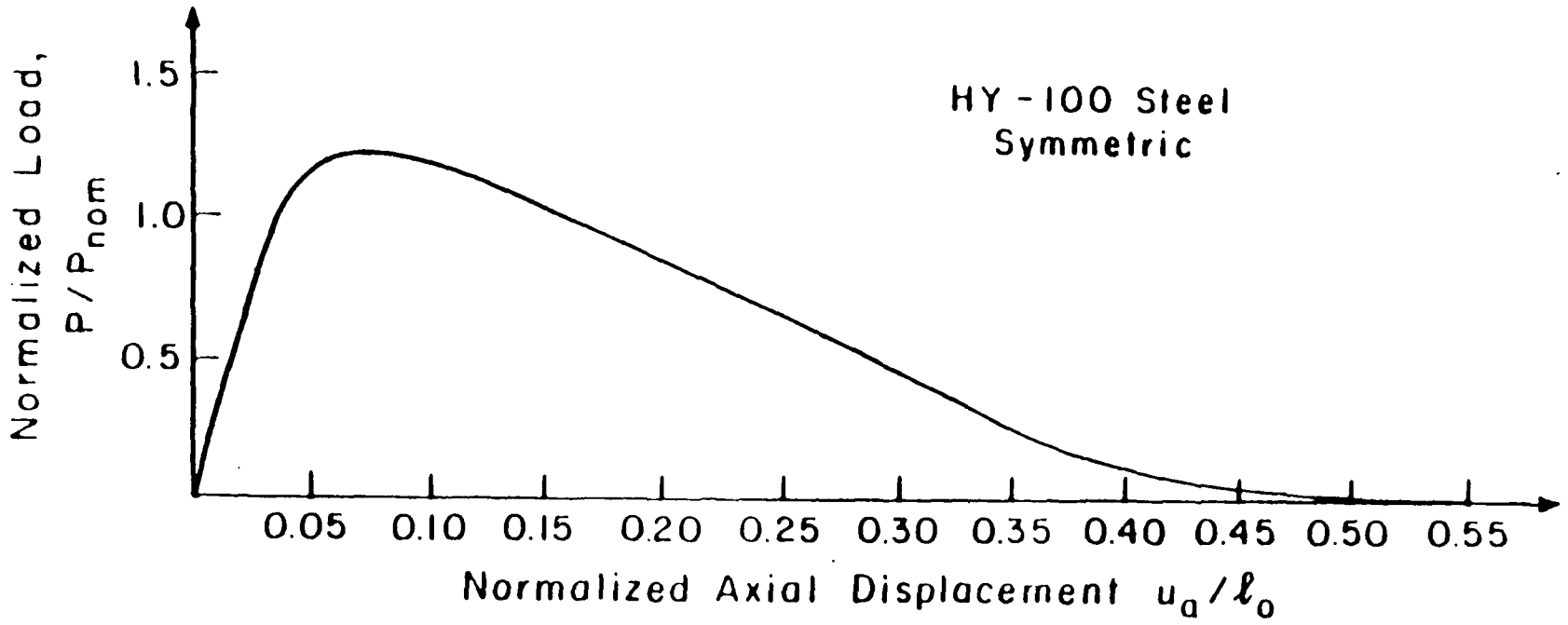

Figure 7b Test Data for the HY-100 Steel Symmetric Specimens

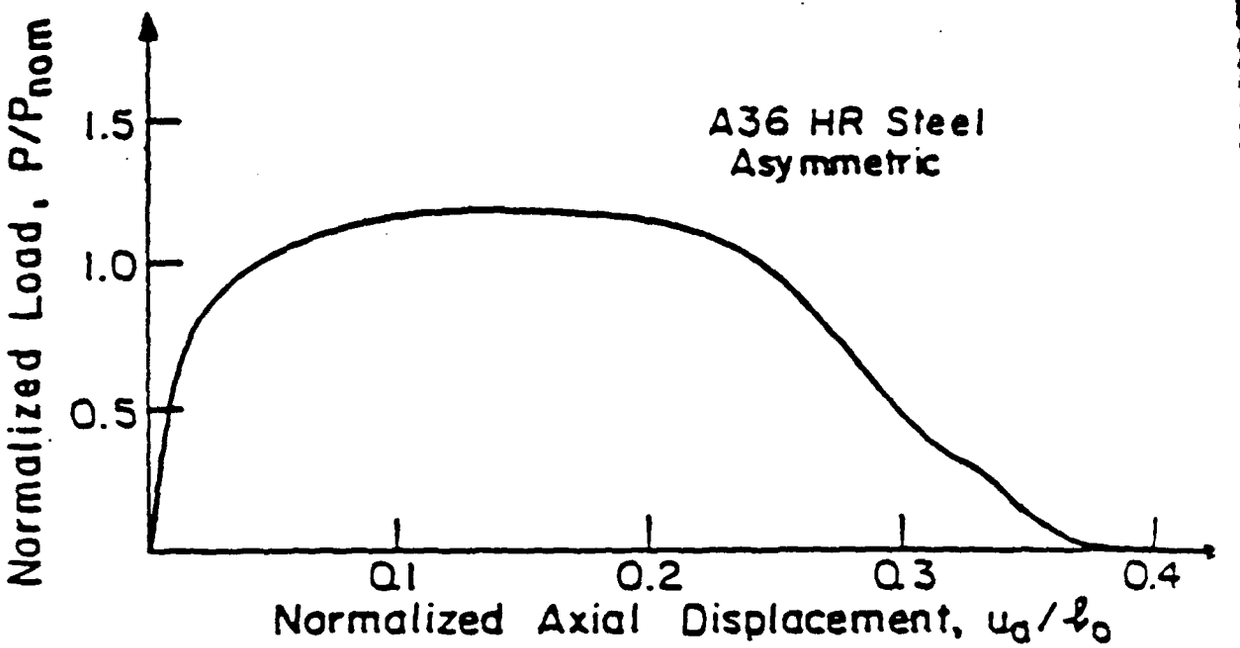

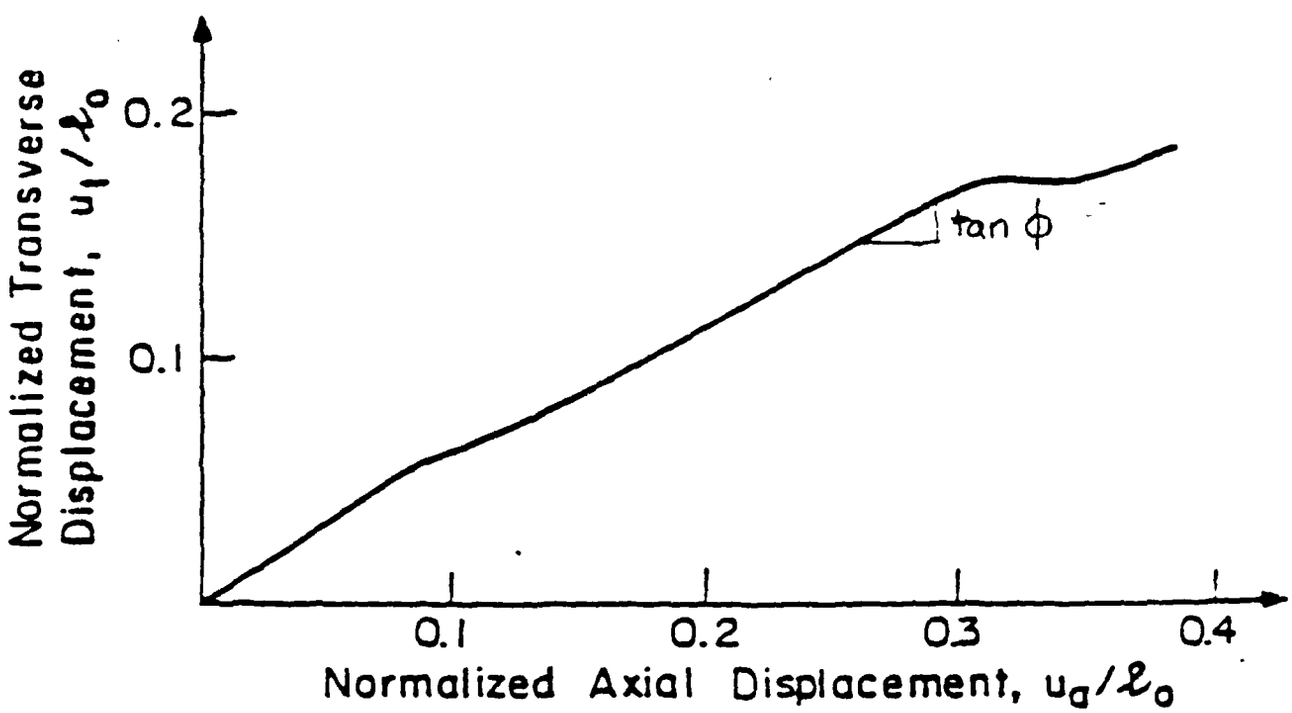

Figure 8a Test Data for the A36 Hot Rolled Steel Asymmetric Specimens

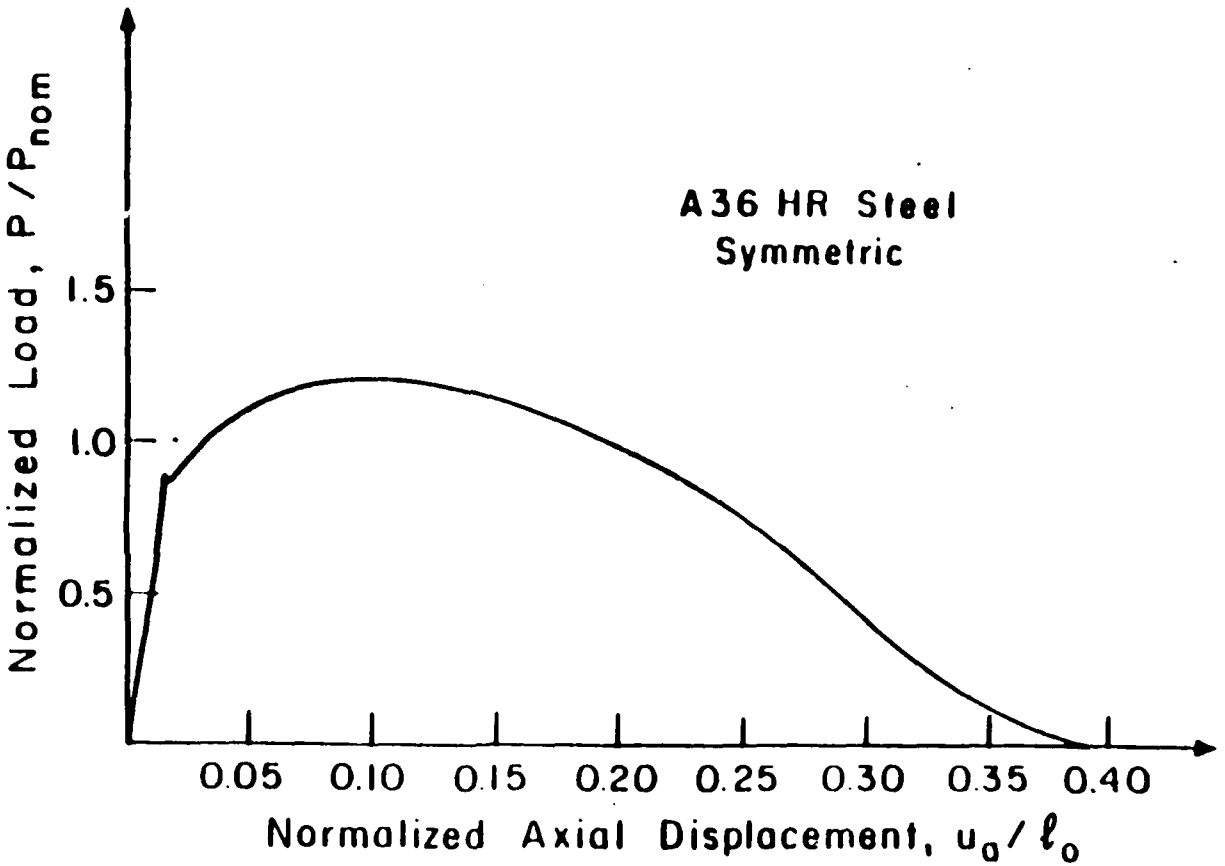

Figure 8b Test Data for the A36 Hot Rolled Steel Symmetric Specimens

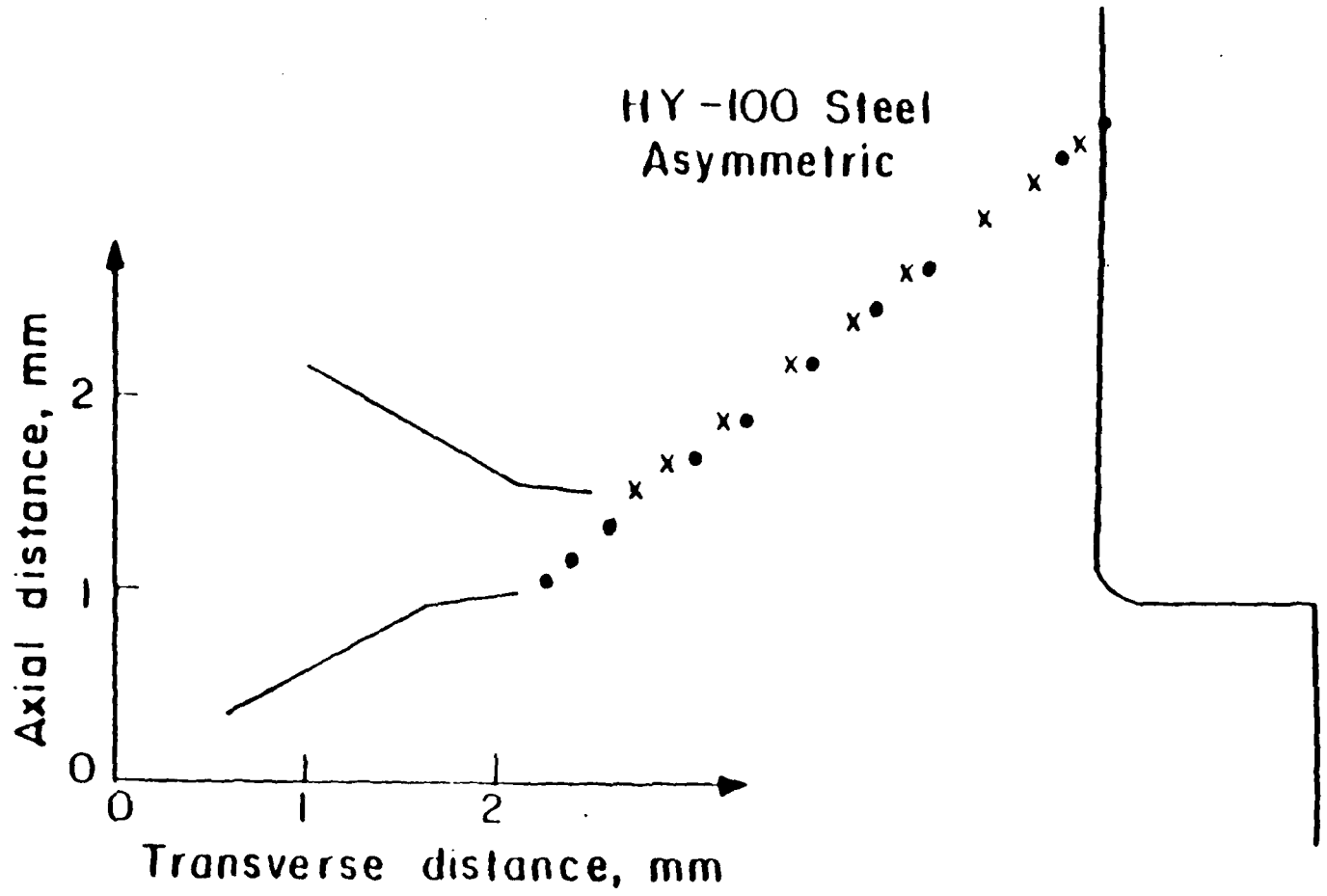

Figure 9a Fracture Surface Profile for the HY-100 Steel Asymmetric Specimens

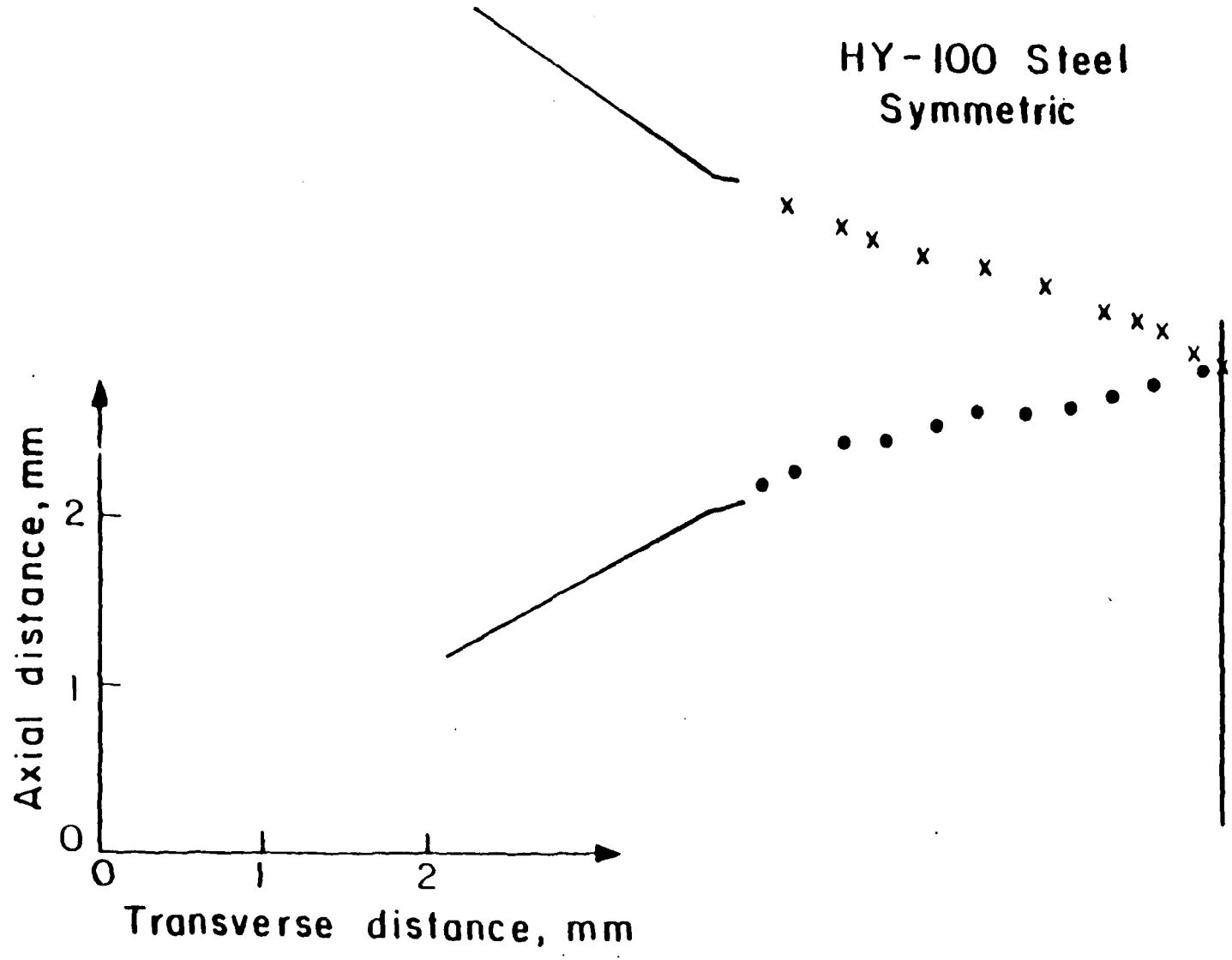

Figure 9b Fracture Surface Profile for the HY-100 Steel Symmetric Specimens

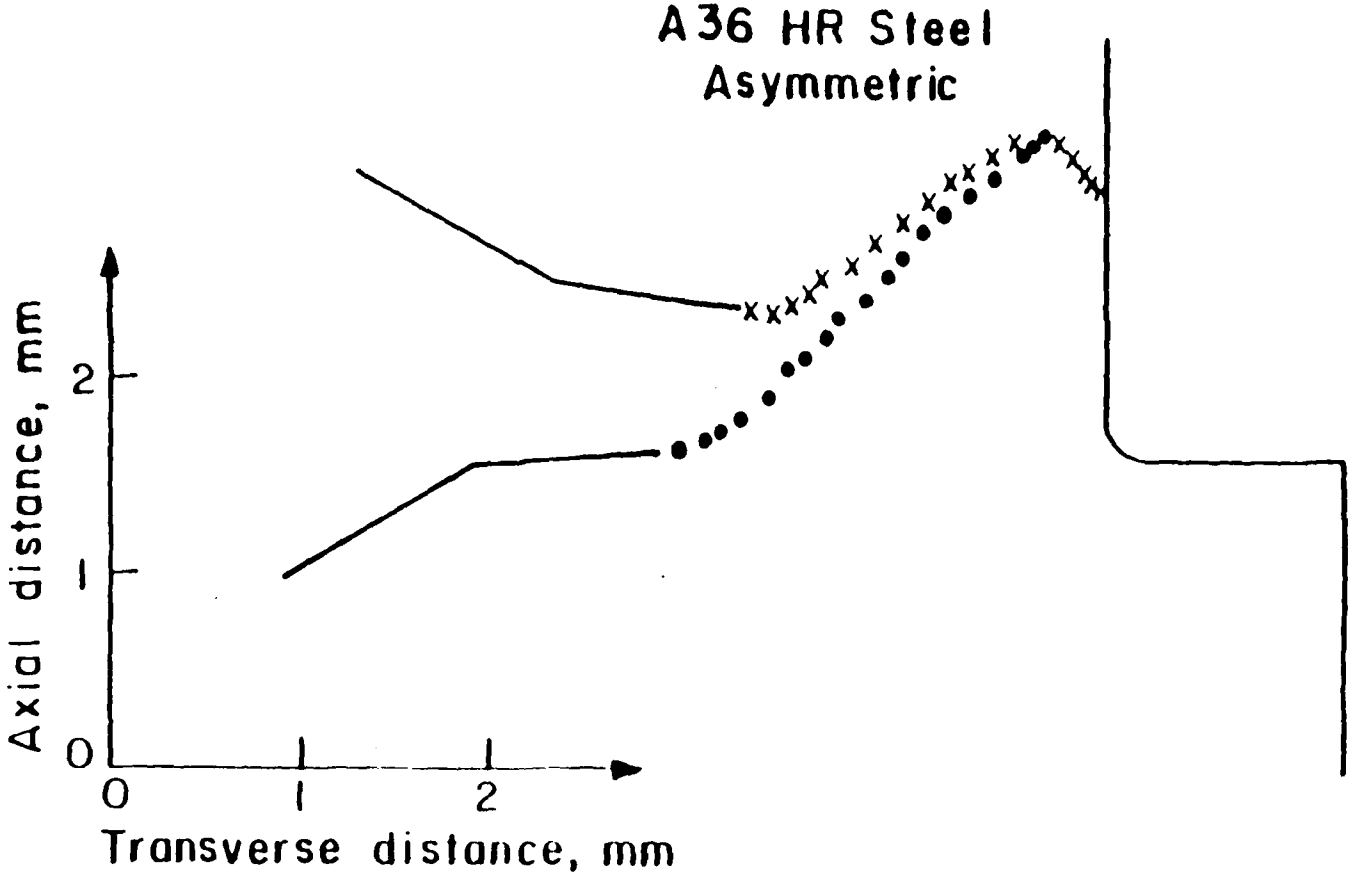

Figure 10a Fracture Surface Profile for the A36 Hot Rolled Steel Asymmetric Specimens

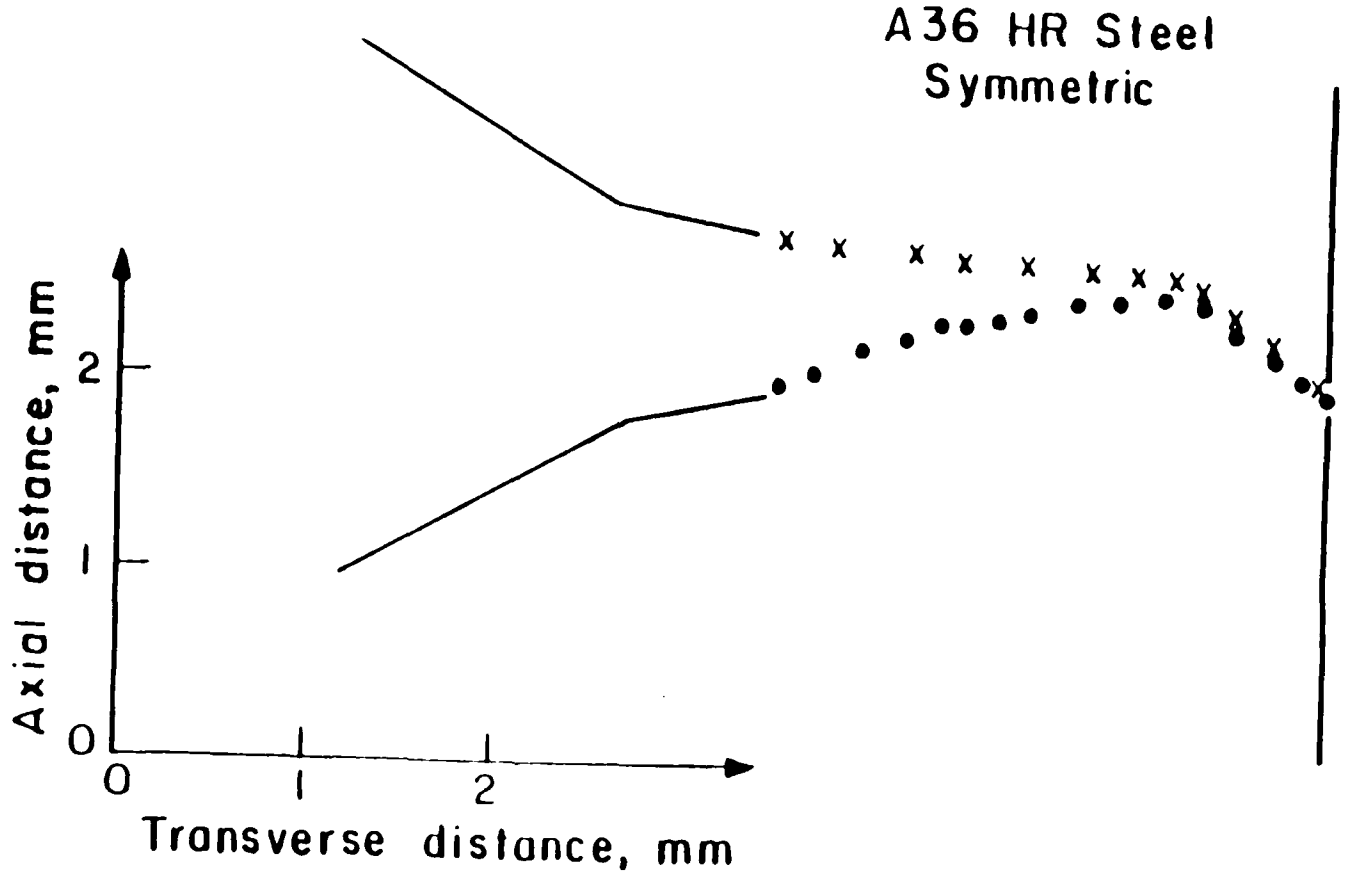

Figure 10b Fracture Surface Profile for the A36 Hot Rolled Steel Symmetric Specimens

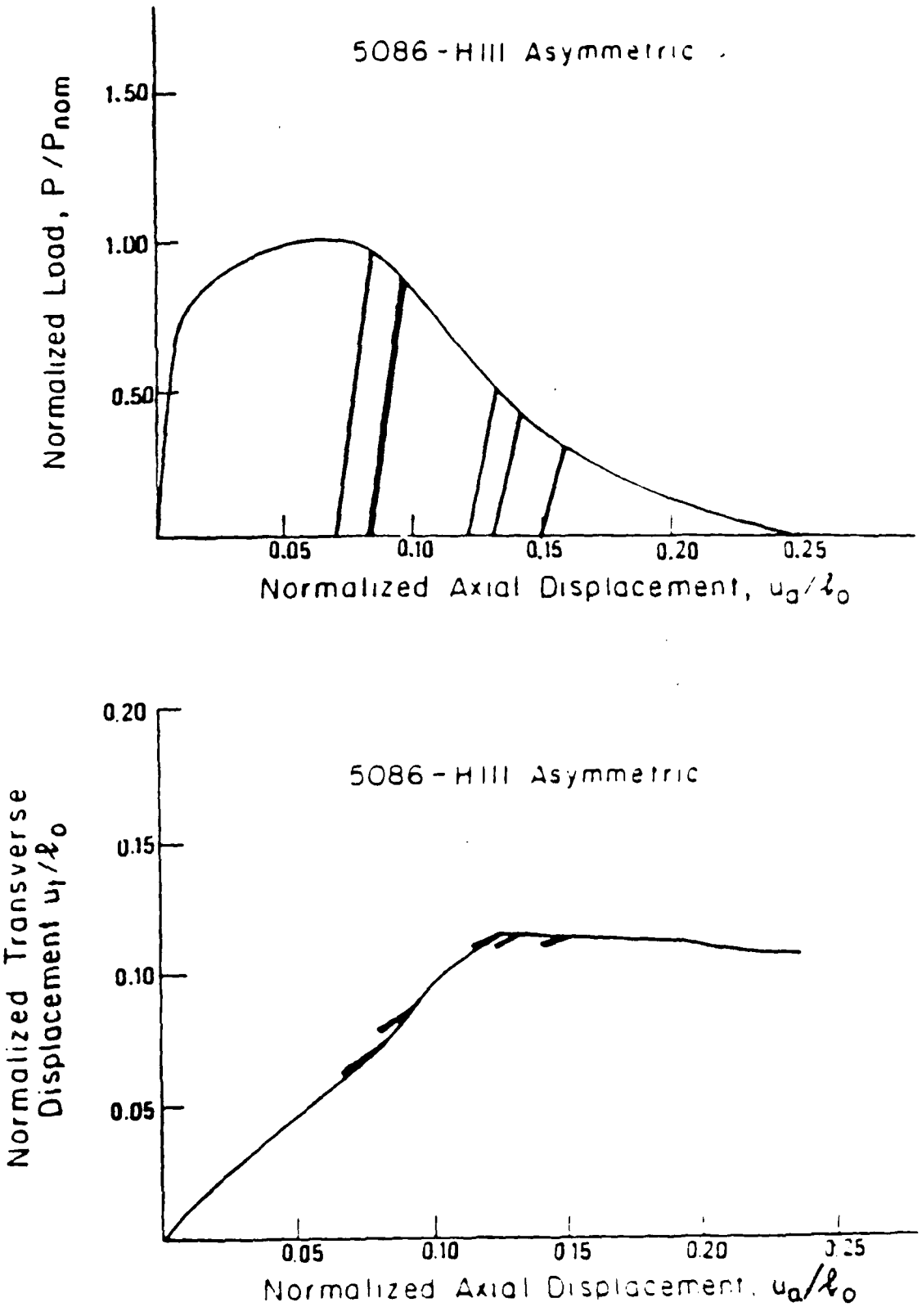

Figure 11a Test Data for the 38 1 mm dia 5086-H111 asymmetric specimens showing the unloading-loading points for marking the crack front

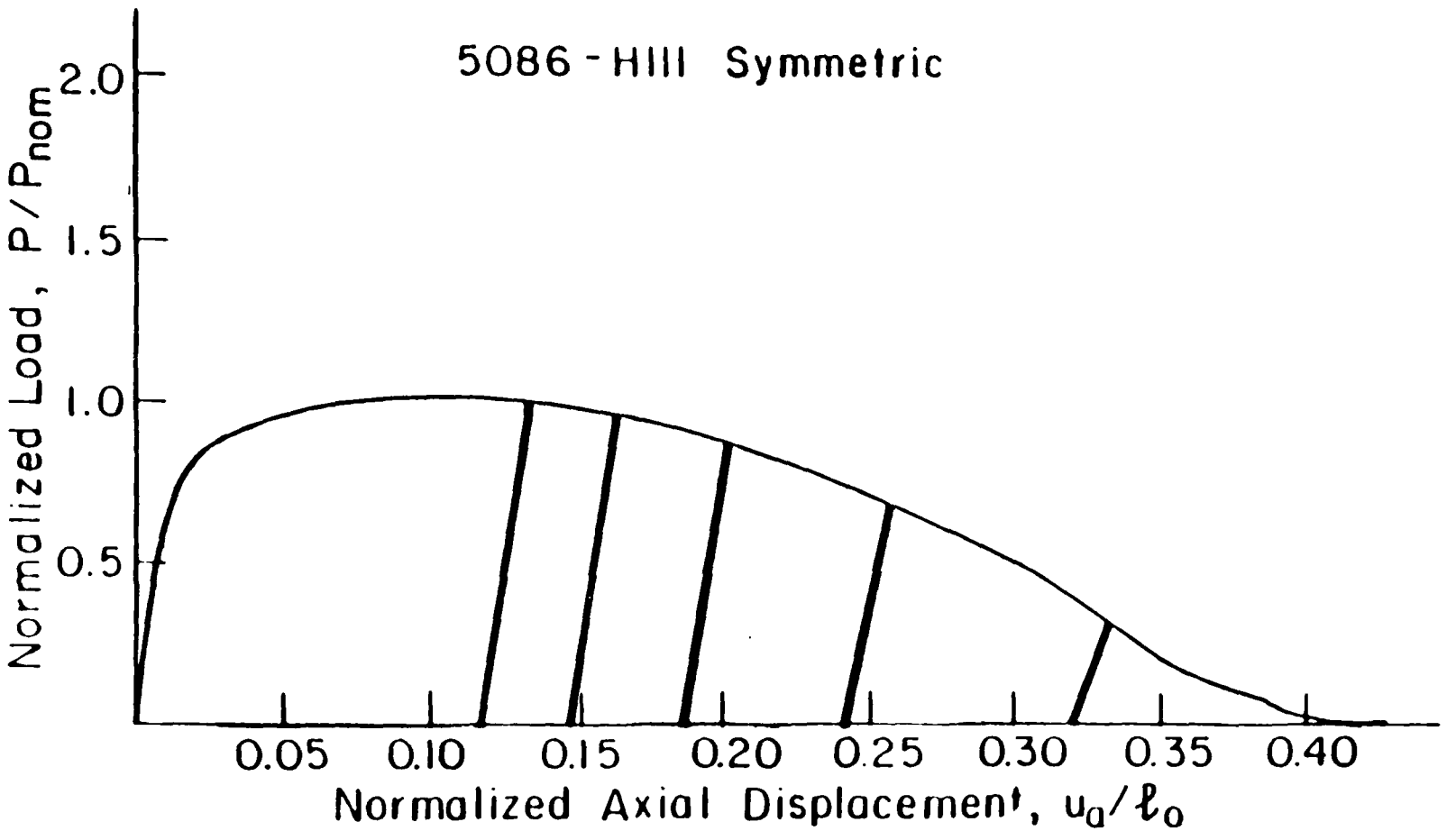

Figure 11b Test Data for the 38 1 mm dia 5086-H111 symmetric specimens showing the unloading-loading points for marking the crack front

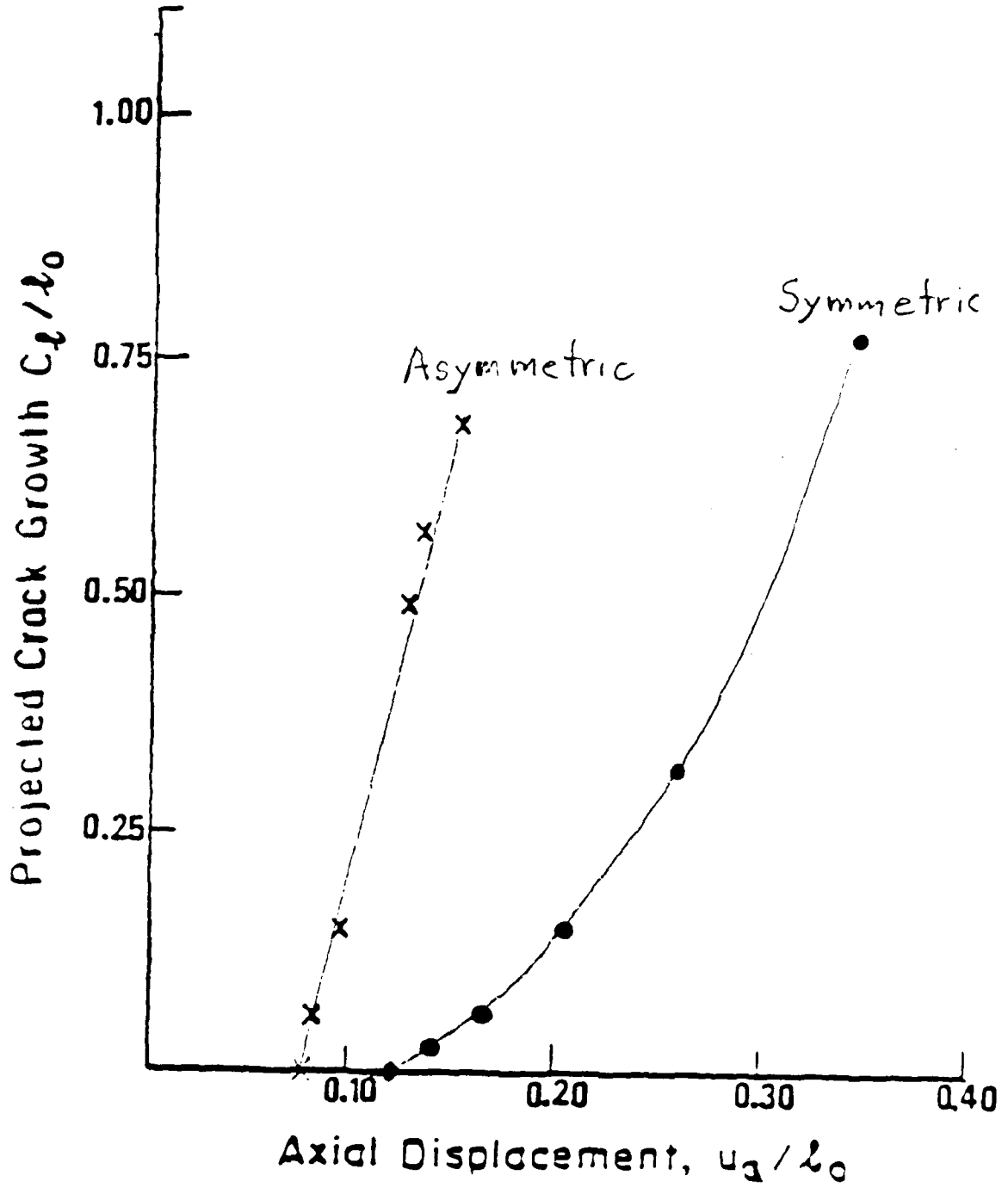

Figure 12 Crack advance-displacement data for the specimens of Figs 11a, 11b The fatigue marks provided the crack positions

END

DTIC

9-86